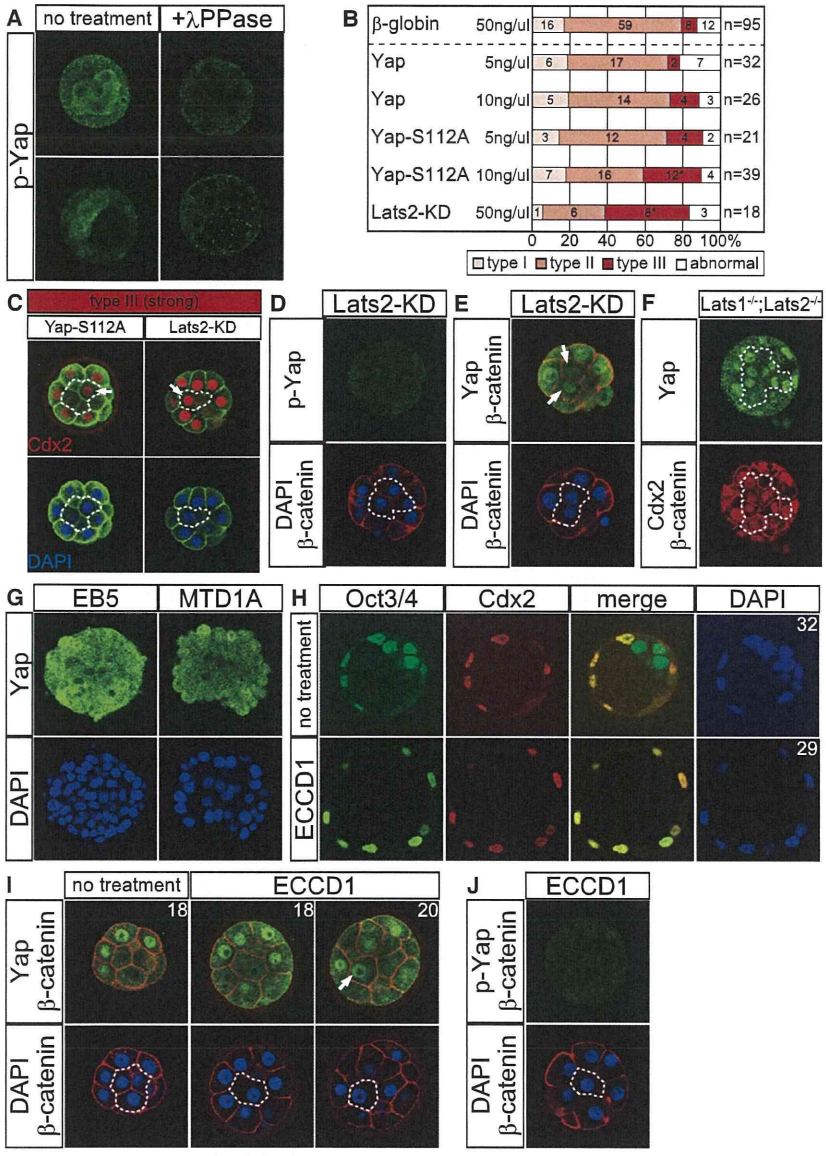

Figure 6. Cell Adhesion and Lats2 Suppress Nuclear Yap Localization in Inside Cells

(A) Immunofluorescence localization of phosphorylated Yap (p-Yap) in preimplantation embryos. A stronger p-Yap signal was detected in inside cells of morula-stage embryos and in the inner cell masses of blastocyst-stage embryos. Treatment with lambda protein phosphatase (λPPase) eliminated p-Yap from inside cells.

(B) Graph summarizing the effects of *Yap-S112A* or *Lats2-KD* on Cdx2 expression in inside cells. The asterisks indicate that the differences were significant compared to the control β-globin-injected group.

(C) Representative embryos showing the effects of injection of *Yap-S112A* or *Lats2-KD* on Cdx2 expression (red). Membrane and nuclei were counterstained with green and blue, respectively.

(D and E) Representative embryos showing reduction of the (D) p-Yap signal and (E) increased nuclear Yap in embryos injected with *Lats2-KD* RNA.

(F) A representative *Lats1*$^{-/-}$; *Lats2*$^{-/-}$ embryo showing increased nuclear Yap and strong Cdx2 expression in the inner cells.

(G) Immunofluorescence localization of Yap in cell aggregates of two cell lines, EB5 (ES) and MTD1A.

(H) Representative embryos after treatment with an anti-E-Cadherin antibody, ECCD1 (bottom).

(I) Altered Yap localization in ECCD1-treated embryos. ECCD1-treated embryos, which failed to exclude Yap from nuclei (center) or exhibited obvious nuclear accumulation of Yap (right) (embryo cell number indicated).

(J) Levels of p-Yap in ECCD1-treated embryos.

suggest that Yap phosphorylation leads to its cytoplasmic localization in inside cells of the preimplantation embryo.

We next examined factors regulating Yap localization during TE formation. In cultured cells, Hippo signaling suppresses the nuclear accumulation of Yap through the activities of Lats1 and Lats2 (Dong et al., 2007; Hao et al., 2008; Ota and Sasaki, 2008; Zhang et al., 2008a; Zhao et al., 2007). We examined localization of Yap in embryos after *Lats2* overexpression. As expected, *Lats2* overexpression greatly reduced nuclear Yap accumulation (Figure 5H). Moreover, Cdx2 levels were also significantly downregulated in these embryos (Figures 5F and 5G), consistent with a requirement for nuclear Yap localization in Cdx2 expression. *Lats2*-injected embryos also failed to form blastocoels after extended culture (data not shown), also characteristic of *Tead4*$^{-/-}$ embryos (Nishioka et al., 2008), consistent with a loss of Yap/Tead activity in both situations. Importantly, *Lats2* overexpression did not dramatically alter cell number, compared with control embryos, suggesting that the effects of *Lats2* on Yap localization and Cdx2 levels were not an artifact of altered developmental timing (Figures 5F and 5H and data not shown). By contrast, overexpression of a Lats-related kinase, Ndr1 (Stk38), had no effect on Cdx2 expression (Figure 5G), indicating specificity of the *Lats2* overexpression phenotype. Taken together, these observations suggest a model in which *Lats* kinases restrict Yap-dependent Tead4 activity to outside cells of the embryo to restrict Cdx2 expression to the nascent TE.

Given that Yap phosphorylation regulates its localization and activity, we reasoned that a phosphorylation-defective Yap would have enhanced Cdx2-inducing activity. To test this, we overexpressed *Yap-S112A* (Figure 4A). Injection of low doses (5 ng/μl and 10 ng/μl) of *Yap-S112A* RNA led to dose-dependent and significant increases in type III embryos with elevated Cdx2 expression and was more effective than wild-type *Yap* at these doses (Figures 6B and 6C). These observations support the proposal that Lats-mediated changes in Yap phosphorylation can alter the Cdx2-inducing activity of Yap during preimplantation development.

Next, we examined the requirement for Lats in the regulation of Yap localization during preimplantation development. The mouse has two *Lats* genes, both of which are expressed throughout preimplantation development (Figure 3A). Since null mutations in either gene do not disrupt preimplantation development (McPherson et al., 2004; St. John et al., 1999; Yabuta et al., 2007), we overexpressed a catalytically inactive (kinase dead; KD) variant of Lats2, designed to dominantly inhibit both Lats1 and Lats2. As predicted, embryos overexpressing *Lats2-KD* exhibited clearly reduced p-Yap levels (Figure 6D), as well as Yap accumulation in nuclei of inside cells (Figure 6E) and a significant increase in Cdx2 in inside cells (type III embryos) (Figures 6B and 6C). Finally, to genetically explore the role of Lats1/2, we generated a null allele of *Lats1*, and we examined embryos obtained from intercrossing *Lats1*$^{+/-}$; *Lats2*$^{+/-}$ mice. Consistent with the analysis of *Lats2-KD* overexpression, *Lats1*$^{-/-}$; *Lats2*$^{-/-}$ double mutant embryos exhibited nuclear accumulation of Yap and strong Cdx2 expression in inside cells (n = 6/7) (Figure 6F; Figure S2). Taken together, these observations strongly suggest that Lats1/2 regulate Yap localization during preimplantation development.

Cell-Cell Contact Inhibits Nuclear Accumulation of Yap in Inside Cells

In cultured cells, the subcellular localization of Yap and therefore Tead activity are controlled by cell-cell contacts via the Hippo signaling pathway (Ota and Sasaki, 2008; Zhao et al., 2007). We therefore asked whether cell contact is also involved in the regulation of Yap localization in preimplantation embryos. To examine whether the degree of cell-cell contact can regulate the subcellular localization of Yap in three-dimensional cell aggregates, we first examined its localization in cultured aggregates of a mouse ES cell line, EB5. Yap was detected only in the cytoplasm of cells internal to the aggregates, whereas Yap was detected in the nucleus and cytoplasm of outer cells of aggregates (Figure 6G, left). Similar results were obtained for aggregates of an epithelial cell line, MTD1A (Figure 6G, right). These correlative results suggest that circumferential cell contacts may inhibit the nuclear localization of Yap.

We next disrupted E-cadherin-mediated cell adhesion by using the E-cadherin blocking antibody ECCD1. As reported (Shirayoshi et al., 1983), treatment of compacted 8-cell embryos with ECCD1 led to decompaction. Culture of these embryos led to the reestablishment of cell adhesion, recompaction, and blastocoel formation, although the timing of this latter process was premature, resulting in ICM sizes that were either small or undetectable (Figure 6H; Figure S3; data not shown) (Shirayoshi et al., 1983). As expected based on the severe reduction of ICM in older ECCD1-treated embryos, Yap was not strictly excluded from nuclei of inside cells among ECCD1-treated embryos examined shortly after recompacting (18- to 22-cell stages, n = 6/8) (Figure 6I, middle). In fact, inside cells exhibited levels of nuclear Yap comparable to those of outside cells in some embryos (n = 2/8) (Figure 6I, right). Conversely, p-Yap levels were clearly reduced in inside cells of ECCD1-treated embryos (Figure 6J). Thus, continuous maintenance of circumferential cell-cell contact or adhesion is a prerequisite for the proper regulation of Yap phosphorylation and repression of Yap accumulation in the nuclei of inside cells.

Cell Position Can Regulate Yap Localization and Cell Fate

The observation that the degree of cell contact correlates with Yap localization and activity provided a potential link between embryo topology and cell fate specification. To test this hypothesis, we examined Yap localization and Cdx2 expression after the manipulation of cell position, by using two different approaches. First, we forced cells to occupy an inside position in reaggregated embryos. Embryos were dissociated at the 8-cell stage, a stage at which Yap is nuclear in all cells, and prior to the creation of inside cells. In nondissociated 8-cell embryos, apicobasal cell polarization can be visualized by examining Ezrin, which localizes to the apical cell pole (Louvet-Vallee et al., 2001). However, in individual 1/8 blastomeres, this pattern was lost, as was nuclear Yap (Figure 7A). Next, we aggregated individual blastomeres from three different embryos into one large chimera, with some cells now occupying a position internal to the others. In these reaggregated embryos, outside cells reestablished polarity, and nuclear Yap and Cdx2 were detected. In contrast, neither nuclear Yap nor Cdx2 were detected in inside cells (Figure 7B).

As a second approach to manipulating cell position, we examined the dynamics of Yap localization and Cdx2 expression in the regenerating TE after immunosurgery (Rossant and Lis, 1979; Spindle, 1978). After immunosurgery, most embryos had reestablished a morphologically distinct TE layer and blastocoel by 24 hr (n = 4/7), and nuclear Yap and Cdx2 were detected in outside cells of all regenerates (Figure 7C, n = 7/7). At 12 hr after immunosurgery, some cells appeared to be flattening on the surface of the ICM (n = 5/5), and nuclear Yap and Cdx2 were detected in these cells, although levels were apparently weaker compared with levels seen in later stages of regeneration (Figure 7D, n = 4/5). Together, these observations support the hypothesis that cell position influences the cell fate in preimplantation embryos by regulating subcellular localization of Yap.

DISCUSSION

Tead4 Instructively Regulates Multiple Transcription Factors to Promote Trophoblast Development

Although *Tead4* is required for *Cdx2* expression in vivo, the unpatterned expression of *Tead4* (Nishioka et al., 2008) made it difficult to predict that Tead4 restricts Cdx2 expression to outside cells during TE formation. We have shown that the activity of Tead4 is regulated, and that its activation is sufficient to regulate multiple factors in parallel to promote trophoblast fate specification in the ES cell model (Figure 7E). These observations are consistent with our analysis of *Tead4* mutant embryos (Nishioka et al., 2008), and with the fact that the *Tead4* mutant phenotype is more severe than loss of *Cdx2* alone (Strumpf et al., 2005). Thus, Tead4 appears to act at the top of a hierarchy of trophoblast-specific transcription factors, among which *Cdx2* plays a central role. However, we do not yet know whether Tead4 regulates *Cdx2* directly, since the *Cdx2* trophoblast enhancer has not been identified. Whereas Tead4-Yap activates Cdx2 in the outer cells, the uniform expression of Oct3/4 up to the late blastocyst stage would suggest that *Cdx2* receives persistent suppressive input from Oct3/4 (Dietrich and Hiiragi, 2007; Niwa et al., 2005). Tead4 may, therefore, promote Cdx2

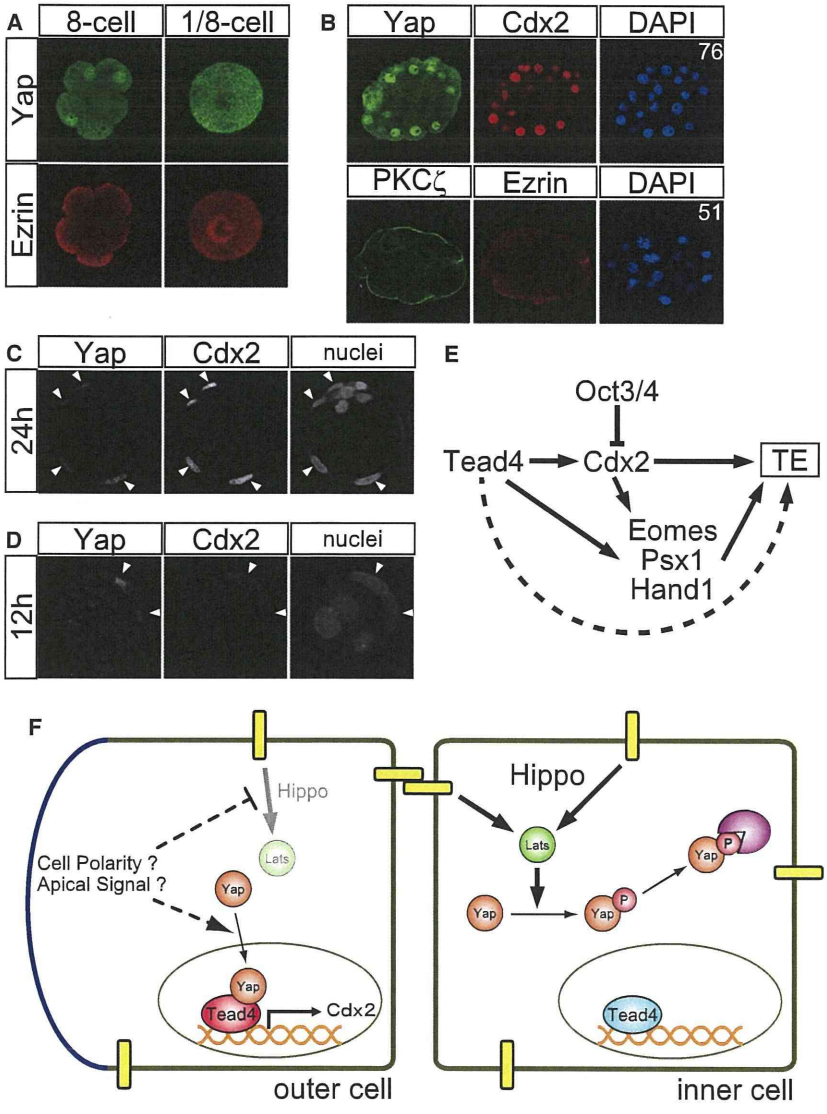

Figure 7. Cell Position Controls Nuclear Localization of Yap

(A) Altered Yap localization and cell polarity (Ezrin) in dissociated blastomeres of the 8-cell embryo.

(B) Localization of Yap, PKCζ, and Ezrin in reaggregated embryos.

(C and D) Yap localization and Cdx2 expression in isolated inner cell masses (C) 24 hr and (D) 12 hr after immunosurgery. Arrowheads indicate Yap-positive nuclei.

(E) A model of the transcriptional network regulating TE development.

(F) A model of cell position-dependent fate specification in preimplantation embryos. See Discussion for details.

expression by overcoming this negative input. Thus, Tead4 instructively regulates multiple transcription factors to promote trophoblast development.

Lats and Yap Convert Positional Information into Cell Fate Information

Two classical models of cell fate specification during preimplantation development are the Inside-Outside Model, in which, topological differences dictate cell fates (Tarkowski and Wroblewska, 1967), and the Polarity Model, wherein differential inheritance of information present along the apicobasal axis dictates both cell position and fate (Johnson and Ziomek, 1981). These models are not mutually exclusive and provide a framework for interpreting our results (Figure 7F). As we have shown, two components of the Hippo signaling pathway, Lats and Yap, are involved in the establishment of position-dependent Tead4 activity and cell fate specification. In inside cells, Yap is phosphorylated by Lats and is excluded from the nuclei. As a consequence, Tead4 remains inactive, and these cells adopt an ICM fate. In the outside cells, lower levels of Yap phosphorylation allow for its nuclear accumulation, which leads to activation of Tead4. In turn, active Tead4 induces trophoblast genes, including *Cdx2*, and promote TE fate.

Although cell position appears to influence Yap localization, the exact mechanisms underlying this phenomenon remain elusive. One likely mechanism is the difference in the degree of cell-cell contacts. Inside cells are surrounded entirely by outside cells, whereas outside cells have an outside-exposed surface. Thus, the degree of cell contact could influence Lats- and/or Hippo-mediated cell signaling. Cell contact-based changes in Hippo signaling have been proposed to explain cell contact-mediated inhibition of proliferation in cultured cells (Ota and Sasaki, 2008; Zhao et al., 2007), and cell contacts are actually required for the suppression of nuclear Yap in inside cells of preimplantation embryos.

Although our observations generally support the Inside-Outside model of early lineage specification, they do not rule out involvement of the Polarity Model. In addition to cell-cell contact, other information, such as cell polarization or the presence of an exposed apical surface, may also contribute to differential Yap localization in the early embryo, for example by restricting the localization or activity of Hippo signaling components. In support of this, dissociated blastomeres, which do not receive cell contact information and also lose polarity, did not exhibit nuclear Yap. As two transmembrane receptors, Fat and CD44, are known upstream regulators of Hippo signaling (Bennett and Harvey, 2006; Hamaratoglu et al., 2006; Morrison et al., 2001; Silva et al., 2006; Willecke et al., 2006), it is tempting to speculate that signaling through these proteins may transmit cell contact information to Lats/Yap in preimplantation embryos.

Although recently it has been shown that Ras-MAPK signaling promotes TE development (Lu et al., 2008), its relationship to Tead4-Yap remains unknown. Interestingly, MAPK signaling negatively regulates Tead activity in cultured cells (Thompson et al., 2003).

Our model places importance on the suppression of Tead4 activity in inside cells to establish differential Tead4 activity along the inside-outside axis. Active Tead4 induces and/or reinforces *Cdx2* expression, overcoming Oct3/4-mediated repression in outside cells, whereas inactive Tead4 together with Oct3/4 may suppress *Cdx2* expression in inside cells. Inactive Tead4 likely acts as a repressor and suppresses *Cdx2* expression, as switching roles between activator and repressor is a typical feature of transcription factors at the end of signaling pathways (Barolo and Posakony, 2002). Continuous operation of this mechanism throughout preimplantation development likely ensures position-dependent cell fate specification, whereas inside and outside daughters are produced from mothers that are initially outside (Fleming, 1987). This system would confer a degree of developmental flexibility on preimplantation mouse embryos. Recently identified asymmetric distribution of *Cdx2* mRNA (Jedrusik et al., 2008) may also be involved in this process.

A Role for Hippo Signaling in Preimplantation Embryos

The Hippo signaling pathway mediates cell contact-mediated growth inhibition in cultured cells (Lei et al., 2008; Ota and Sasaki, 2008; Zhao et al., 2007, 2008), but our evidence suggests a slightly different role during preimplantation development. Although cell contact is still involved, growth inhibition is not, since changes in Yap localization suppressed Cdx2 expression without affecting cell number. A similar role in cell fate specification has been observed in *Drosophila* photoreceptor differentiation (Mikeladze-Dvali et al., 2005), suggesting that Hippo signaling may regulate distinct cellular outcomes, depending on the context.

EXPERIMENTAL PROCEDURES

Cell Culture

EB5 ES cells were cultured on gelatin-coated dishes in the absence of feeder cells in ES medium (Glasgow modification of Eagle's medium (GMEM) supplemented with 10% (v/v) FCS, 1000 U/ml LIF, 1× sodium pyruvate, 1× nonessential amino acids, 10^{-4} M β-mercaptoethanol) (Niwa et al., 1998) containing 10 μg/ml blasticidin S. 5ECER4 ES cells (Niwa et al., 2005) were cultured in ES medium containing 10 μg/ml blasticidin S and 1 μg/ml puromycin. To establish ES cells stably expressing Tead4VP16ER (5TVER7 and 5TVER16), EB5 ES cells were electroporated with linearized pCAG-Tead4VP16ER-IP and were selected with 1 μg/ml puromycin in ES cell medium containing 10 μg/ml blasticidin S. *Tead4*$^{-/-}$ ES cells and derivatives were maintained in serum-free CultiCell medium (Stem Cell Sciences, Japan) (Ogawa et al., 2004). To establish *Tead4*$^{-/-}$ ES cells stably expressing Cdx2ER (T4CER9 and T4CER10), *Tead4*$^{-/-}$ ES cells (#1–5) (Nishioka et al., 2008) were electroporated with linearized pCAG-Cdx2ER-IP (Niwa et al., 2005) and were selected with 1 μg/ml puromycin in CultiCell serum-free ES medium. To establish *Cdx2*$^{-/-}$ ES cells stably expressing Tead4VP16ER (CTVER5 and CTVER20), dko23-5 ES cells (Niwa et al., 2005) were electroporated with linearized pCAG-Tead4VP16ER-IP and selected with 1 μg/ml puromycin in ES cell medium containing 10 μg/ml blasticidin S and 200 μg/ml G418. In dko23-5 ES cells, expression of *Oct3/4* does not change during differentiation, because *Oct3/4* is expressed from a transgene (Niwa et al., 2005). To induce transgenes, 5ECER4, T4CER9, and T4CER10 were induced with 1 μg/ml tamoxifen in ES medium. 5TVER7 and 5TVER16 were induced with 0.1 μg/ml tamoxifen, and CTVER5 and CTVER20 were induced with 0.2 μg/ml tamoxifen; higher doses of tamoxifen resulted in significant cell death of 5TVER7, 5TVER16, CTVER5, and CTVER20. Induction of ES cell differentiation into TS cells was performed as previously described (Niwa et al., 2005).

ES cell transfection with siRNA was performed by using Lipofectamine 2000 as previously described (Hough et al., 2006), by using feeder-free conditions. For Oct3/4 knockdown, three predesigned Stealth siRNAs (Stealth Select RNAi) targeting *Oct3/4* (Pou5f1-MSS237605, Pou5f1-MSS237606, and Pou5f1-MSS237607) were obtained from Invitrogen. Pou5f1-MSS237605 and Pou5f1-MSS237606 clearly reduced *Oct3/4*, whereas Pou5f1-MSS237607 exhibited a weaker effect. The two former siRNAs were therefore used and produced similar results. The representative result with Pou5f1-MSS237605 siRNA is shown in a figure. The Stealth RNAi Negative Control Medium GC Duplex (Invitrogen) was used for control experiments.

MTD1A (Hirano et al., 1987), NIH 3T3, and HeLa cells were cultured in Dulbecco's Modified Eagle's Medium containing 10% Fetal Calf Serum (DMEM + 10% FCS).

For detailed information about plasmids, see Supplemental Data.

Luciferase Assay

NIH 3T3 or HeLa cells were seeded at a density of 1×10^5 cells/well on 12-well plates 24 hr before transfection. A DNA mixture consisting of effector (50 ng), pCMV-Gal4 (BD) or pCMV-Gal4-Tead4C (50 ng), pG4-TK-Luc (200 ng), and pCS2-β-gal (50 ng) were transfected for 24 hr with 2 μl FuGENE HD (Roche). Lysate preparation, luciferase, and β-galactosidase assays were performed as described (Sasaki et al., 1999). Luciferase activities were normalized to β-galactosidase activities. For each experiment, values from two samples were averaged and are presented with standard errors.

RT-PCR

Total RNA was isolated from ES cells or embryos by using Trizol reagent (Invitrogen) by following the manufacturer's instruction. cDNA was prepared from 1 μg total RNA by using Ready-To-Go You-Prime First-Strand Beads (GE Healthcare) or Superscript III reverse transcriptase (Invitrogen) and Oligo-dT primers (Invitrogen) per manufacturers' instructions. cDNA was diluted 1:200 for quantitative PCR reactions. Primers and conditions for Quantitative-PCR (Q-PCR) reactions for *Cdx2*, *Eomes*, *Psx1*, *Hand1*, *Itga7*, *Oct3/4*, *Sox2*, *Fgf4*, and *Gapdh* are described by Niwa et al. (2005). Q-PCR was performed by using SYBR Premix Ex Taq (Takara Bio, Kyoto Japan) and an ABI PRISM 7900HT (Applied Biosystems). Expression of each gene was normalized to the expression of *Gapdh*. Average results and standard errors from three independent measurements are presented.

Mouse Lines

Wild-type litters were obtained by crossing C57BL/6 and [C57BL/6xDBA]F1 mice. *Yap*^{tm1Smil} mice (Morin-Kensicki et al., 2006) were crossed with *Actb:Cre* transgenic mice to remove the neomycin cassette flanked by *loxP* sites. Resulting mice (*Yap*$^{\Delta tm1}$) are referred to as *Yap* mutant mice in this paper. *Wwtr1* mutant mice (*Taz*^{lacZ}) were previously described (Makita et al., 2008). *Lats2* mutant mice were previously described (Yabuta et al., 2007). The *Lats1* mutant allele was generated by homologous recombination in ES cells in H.N.'s laboratory. Exon 1 (E1), containing a translation initiation codon, was replaced with a cassette containing the *Pgk* promoter, the *neomycin resistance* gene, and the *Pgk* polyA signal (Figure S4A), resulting in generation of a null allele. Details for the generation and characterization of *Lats1* mutants will be described elsewhere by N.Y. and H.N. Mice were housed in environmentally controlled rooms in the Laboratory Animal Housing Facility of the RIKEN Center for Developmental Biology, under the institutional guidelines for animal and recombinant DNA experiments.

Embryo Culture and Embryo Manipulation

Embryo culture was performed as previously described (Nishioka et al., 2008). Treatment of embryos with ECCD1 (Takara Bio, Kyoto Japan) was performed as previously described (Shirayoshi et al., 1983). Dissociation of 8-cell-stage embryos was performed as previously described (Dietrich and Hiiragi, 2007), and blastomeres were reaggregated by gentle rocking in U-bottom, MPC-coated 96-well plates (Nunc).

RNA Injection

Poly(A)-tailed RNA was synthesized from cDNAs cloned into the pcDNA3.1-poly(A)83 plasmid (Yamagata et al., 2005), and purified RNAs were injected into both blastomeres of 2-cell-stage embryos according to standard protocols (Hogan et al., 1994). Details of plasmids used are provided in Supplemental Data.

Immunofluorescent Staining

Immunofluorescent staining of embryos was performed by following standard protocols. Inside cells were identified by acquiring Z-series confocal images of the stained embryos with LSM510 META (Zeiss). Embryos were fixed in 4% paraformaldehyde in phosphate-buffered saline (PBS) for 15 min at room temperature, and then washed in PBS + 0.2% goat serum (PBSS) for 5 min. Embryos were subsequently permeabilized with 0.2% Triton X-100 in PBS for 20 min at room temperature, washed in PBSS for 5 min, blocked with 2% goat serum in PBS (blocking solution), and incubated overnight with primary antibodies diluted in blocking solution at 4°C. After washing in PBSS for 5 min, embryos were incubated with the following secondary antibodies diluted in PBSS for 1 hr at room temperature: Alexa Fluor 488 goat anti-rabbit (Molecular Probes, A11034; 1:4000) and/or Alexa Fluor 594 goat anti-mouse (Molecular Probes, A11005; 1:4000). Nuclei were visualized by staining with 4,6-diamidino-2-phenylindole dilactate (DAPI; Molecular Probes, D3571). For detection of p-Yap, all solutions up to primary antibody were supplemented with Phosphatase Inhibitor Cocktail (Nacalai Tesque, Kyoto, Japan) at 1:100. For λPPase treatment, ~10 embryos were incubated with 2000 U Lambda Protein Phosphatase (Sigma P9614) in 100 ml λPPase buffer supplied by the manufacturer at 30°C for 1 hr prior to blocking.

Statistics

Statistical analyses were performed with Prism4 statistical software (GraphPad) by using Fisher's exact probability test. For all comparisons, experimental results were compared with control results (*β-globin*-injected). For experiments shown in Figures 2, 4, and 6, the frequencies of type III embryos were compared. For experiments shown in Figure 5, frequencies of type IV embryos were compared. Statistically significant differences ($p < 0.05$) are indicated by asterisks.

Quantification of Immunofluorescent Signals

Confocal images of the stained embryos were acquired with LSM510 META (Zeiss). Average pixel intensities of the Yap and DAPI in nuclear cross-section were measured by using MetaMorph software (Molecular Devices). Yap nuclear signal values were normalized to the DAPI signal. Average values from multiple embryos are presented with standard deviation.

Immunosurgery

Embryos were harvested around E3.0, zonae pellucida were removed, and embryos were subsequently incubated with nonpreadsorbed rabbit anti-mouse lymphocyte antibody (Cedarlane) diluted 1:8 in KSOM for 25 min in a 37°C incubator. Embryos were washed through five droplets of KSOM and then incubated as described above in anti-rabbit Alexa Fluor 488 (1:400, Molecular Probes) for 15 min. Embryos were again washed in KSOM, and then incubated as described above for 8 min in guinea pig complement (Cedarlane) diluted 1:4 in KSOM, and lysed cells were removed by extensive flushing through a pulled glass needle. Resulting inner cell masses were screened for efficient removal of TE by brief examination of fluorescence signal by fluorescence microscopy. Efficiently lysed ICMs were then incubated in KSOM as described above until the indicated time points, then harvested for immunostaining and confocal analysis as described (Ralston and Rossant, 2008). Antibodies used included rabbit anti-YAP (Cell Signaling; 1:100); mouse anti-Cdx2 (Biogenex; 1:200); anti-mouse Alexa 546, anti-mouse Alexa 488, and Draq5 (Molecular Probes; all at 1:400), and all images were collected during a single confocal session with identical confocal settings.

SUPPLEMENTAL DATA

Supplemental Data include four figures, one table, Supplemental Experimental Procedures, and Supplemental References and can be found with this article online at http://www.cell.com/developmental-cell/supplemental/S1534-5807(09)00077-X.

ACKNOWLEDGMENTS

We thank H. Sato, M. Shibata, and M. Harano for their excellent technical assistance, K. Yamagata for a plasmid, and A. Ogura and K. Mekada for collecting *Lats1/2* mutant embryos. We are also grateful to the Laboratory for Animal Resources and Genetic Engineering for collecting mouse embryos and the housing of the mice. This work was supported by grants from RIKEN (H.S.), by grants-in-aid for Scientific Research (S and B) and for Encouragement of Young Scientists from Ministry of Education, Culture, Sports, Science, and Technology of Japan (N.Y. and H.N.), and by grant #13426 from the Canadian Institutes of Health Research (J.R.).

Received: August 22, 2008
Revised: November 28, 2008
Accepted: February 6, 2009
Published: March 16, 2009

REFERENCES

Barolo, S., and Posakony, J.W. (2002). Three habits of highly effective signaling pathways: principles of transcriptional control by developmental cell signaling. Genes Dev. *16*, 1167–1181.

Basu, S., Totty, N.F., Irwin, M.S., Sudol, M., and Downward, J. (2003). Akt phosphorylates the Yes-associated protein, YAP, to induce interaction with 14-3-3 and attenuation of p73-mediated apoptosis. Mol. Cell *11*, 11–23.

Bennett, F.C., and Harvey, K.F. (2006). Fat cadherin modulates organ size in *Drosophila* via the Salvador/Warts/Hippo signaling pathway. Curr. Biol. *16*, 2101–2110.

Dietrich, J.E., and Hiiragi, T. (2007). Stochastic patterning in the mouse preimplantation embryo. Development *134*, 4219–4231.

Dong, J., Feldmann, G., Huang, J., Wu, S., Zhang, N., Comerford, S.A., Gayyed, M.F., Anders, R.A., Maitra, A., and Pan, D. (2007). Elucidation of a universal size-control mechanism in *Drosophila* and mammals. Cell *130*, 1120–1133.

Fleming, T.P. (1987). A quantitative analysis of cell allocation to trophectoderm and inner cell mass in the mouse blastocyst. Dev. Biol. *119*, 520–531.

Goulev, Y., Fauny, J.D., Gonzalez-Marti, B., Flagiello, D., Silber, J., and Zider, A. (2008). SCALLOPED interacts with YORKIE, the nuclear effector of the hippo tumor-suppressor pathway in *Drosophila*. Curr. Biol. *18*, 435–441.

Hamaratoglu, F., Willecke, M., Kango-Singh, M., Nolo, R., Hyun, E., Tao, C., Jafar-Nejad, H., and Halder, G. (2006). The tumour-suppressor genes NF2/Merlin and Expanded act through Hippo signalling to regulate cell proliferation and apoptosis. Nat. Cell Biol. *8*, 27–36.

Hao, Y., Chun, A., Cheung, K., Rashidi, B., and Yang, X. (2008). Tumor suppressor LATS1 is a negative regulator of oncogene YAP. J. Biol. Chem. *283*, 5496–5509.

Hirano, S., Nose, A., Hatta, K., Kawakami, A., and Takeichi, M. (1987). Calcium-dependent cell-cell adhesion molecules (cadherins): subclass specificities and possible involvement of actin bundles. J. Cell Biol. *105*, 2501–2510.

Hogan, B., Beddington, R., Constantini, F., and Lacy, E. (1994). Manipulating the Mouse Embryo: Laboratory Manual, Second Edition (Cold Spring Harbor, NY: Cold Spring Harbor Laboratory Press).

Hossain, Z., Ali, S.M., Ko, H.L., Xu, J., Ng, C.P., Guo, K., Qi, Z., Ponniah, S., Hong, W., and Hunziker, W. (2007). Glomerulocystic kidney disease in mice with a targeted inactivation of Wwtr1. Proc. Natl. Acad. Sci. USA *104*, 1631–1636.

Hough, S.R., Clements, I., Welch, P.J., and Wiederholt, K.A. (2006). Differentiation of mouse embryonic stem cells after RNA interference-mediated silencing of OCT4 and Nanog. Stem Cells *24*, 1467–1475.

Huang, J., Wu, S., Barrera, J., Matthews, K., and Pan, D. (2005). The Hippo signaling pathway coordinately regulates cell proliferation and apoptosis by inactivating Yorkie, the *Drosophila* homolog of YAP. Cell *122*, 421–434.

Jedrusik, A., Parfitt, D.E., Guo, G., Skamagki, M., Grabarek, J.B., Johnson, M.H., Robson, P., and Zernicka-Goetz, M. (2008). Role of Cdx2 and cell polarity in cell allocation and specification of trophectoderm and inner cell mass in the mouse embryo. Genes Dev. *22*, 2692–2706.

Johnson, M.H., and Ziomek, C.A. (1981). The foundation of two distinct cell lineages within the mouse morula. Cell *24*, 71–80.

Lei, Q.Y., Zhang, H., Zhao, B., Zha, Z.Y., Bai, F., Pei, X.H., Zhao, S., Xiong, Y., and Guan, K.L. (2008). TAZ promotes cell proliferation and epithelial-mesenchymal transition and is inhibited by the hippo pathway. Mol. Cell. Biol. *28*, 2426–2436.

Louvet-Vallee, S., Dard, N., Santa-Maria, A., Aghion, J., and Maro, B. (2001). A major posttranslational modification of ezrin takes place during epithelial differentiation in the early mouse embryo. Dev. Biol. *231*, 190–200.

Lu, C.W., Yabuuchi, A., Chen, L., Viswanathan, S., Kim, K., and Daley, G.Q. (2008). Ras-MAPK signaling promotes trophectoderm formation from embryonic stem cells and mouse embryos. Nat. Genet. *40*, 921–926.

Mahoney, W.M., Jr., Hong, J.H., Yaffe, M.B., and Farrance, I.K. (2005). The transcriptional co-activator TAZ interacts differentially with transcriptional enhancer factor-1 (TEF-1) family members. Biochem. J. *388*, 217–225.

Makita, R., Uchijima, Y., Nishiyama, K., Amano, T., Chen, Q., Takeuchi, T., Mitani, A., Nagase, T., Yatomi, Y., Aburatani, H., et al. (2008). Multiple renal cysts, urinary concentration defects, and pulmonary emphysematous changes in mice lacking TAZ. Am. J. Physiol. *294*, F542–F553.

McPherson, J.P., Tamblyn, L., Elia, A., Migon, E., Shehabeldin, A., Matysiak-Zablocki, E., Lemmers, B., Salmena, L., Hakem, A., Fish, J., et al. (2004). Lats2/Kpm is required for embryonic development, proliferation control and genomic integrity. EMBO J. *23*, 3677–3688.

Mikeladze-Dvali, T., Wernet, M.F., Pistillo, D., Mazzoni, E.O., Teleman, A.A., Chen, Y.W., Cohen, S., and Desplan, C. (2005). The growth regulators warts/lats and melted interact in a bistable loop to specify opposite fates in *Drosophila* R8 photoreceptors. Cell *122*, 775–787.

Morin-Kensicki, E.M., Boone, B.N., Howell, M., Stonebraker, J.R., Teed, J., Alb, J.G., Magnuson, T.R., O'Neal, W., and Milgram, S.L. (2006). Defects in yolk sac vasculogenesis, chorioallantoic fusion, and embryonic axis elongation in mice with targeted disruption of Yap65. Mol. Cell. Biol. *26*, 77–87.

Morrison, H., Sherman, L.S., Legg, J., Banine, F., Isacke, C., Haipek, C.A., Gutmann, D.H., Ponta, H., and Herrlich, P. (2001). The NF2 tumor suppressor gene product, merlin, mediates contact inhibition of growth through interactions with CD44. Genes Dev. *15*, 968–980.

Nishioka, N., Nagano, S., Nakayama, R., Kiyonari, H., Ijiri, T., Taniguchi, K., Shawlot, W., Hayashizaki, Y., Westphal, H., Behringer, R.R., et al. (2005). Ssdp1 regulates head morphogenesis of mouse embryos by activating the Lim1-Ldb1 complex. Development *132*, 2535–2546.

Nishioka, N., Yamamoto, S., Kiyonari, H., Sato, H., Sawada, A., Ota, M., Nakao, K., and Sasaki, H. (2008). Tead4 is required for specification of trophectoderm in pre-implantation mouse embryos. Mech. Dev. *125*, 270–283.

Niwa, H., Burdon, T., Chambers, I., and Smith, A. (1998). Self-renewal of pluripotent embryonic stem cells is mediated via activation of STAT3. Genes Dev. *12*, 2048–2060.

Niwa, H., Miyazaki, J., and Smith, A.G. (2000). Quantitative expression of Oct-3/4 defines differentiation, dedifferentiation or self-renewal of ES cells. Nat. Genet. *24*, 372–376.

Niwa, H., Toyooka, Y., Shimosato, D., Strumpf, D., Takahashi, K., Yagi, R., and Rossant, J. (2005). Interaction between Oct3/4 and Cdx2 determines trophectoderm differentiation. Cell *123*, 917–929.

Ogawa, K., Matsui, H., Ohtsuka, S., and Niwa, H. (2004). A novel mechanism for regulating clonal propagation of mouse ES cells. Genes Cells *9*, 471–477.

Ota, M., and Sasaki, H. (2008). Mammalian Tead proteins regulate cell proliferation and contact inhibition as a transcriptional mediator of Hippo signaling. Development *135*, 4059–4069.

Palmieri, S.L., Peter, W., Hess, H., and Scholer, H.R. (1994). Oct-4 transcription factor is differentially expressed in the mouse embryo during establishment of the first two extraembryonic cell lineages involved in implantation. Dev. Biol. *166*, 259–267.

Pan, D. (2007). Hippo signaling in organ size control. Genes Dev. *21*, 886–897.

Ralston, A., and Rossant, J. (2008). Cdx2 acts downstream of cell polarization to cell-autonomously promote trophectoderm fate in the early mouse embryo. Dev. Biol. *313*, 614–629.

Reddy, B.V., and Irvine, K.D. (2008). The Fat and Warts signaling pathways: new insights into their regulation, mechanism and conservation. Development *135*, 2827–2838.

Rossant, J., and Lis, W.T. (1979). Potential of isolated mouse inner cell masses to form trophectoderm derivatives in vivo. Dev. Biol. *70*, 255–261.

Sasaki, H., Nishizaki, Y., Hui, C., Nakafuku, M., and Kondoh, H. (1999). Regulation of Gli2 and Gli3 activities by an amino-terminal repression domain: implication of Gli2 and Gli3 as primary mediators of Shh signaling. Development (Cambridge, England) *126*, 3915–3924.

Saucedo, L.J., and Edgar, B.A. (2007). Filling out the Hippo pathway. Nat. Rev. Mol. Cell Biol. *8*, 613–621.

Sawada, A., Kiyonari, H., Ukita, K., Nishioka, N., Imuta, Y., and Sasaki, H. (2008). Redundant roles of Tead1 and Tead2 in notochord development and the regulation of cell proliferation and survival. Mol. Cell. Biol. *28*, 3177–3189.

Shirayoshi, Y., Okada, T.S., and Takeichi, M. (1983). The calcium-dependent cell-cell adhesion system regulates inner cell mass formation and cell surface polarization in early mouse development. Cell *35*, 631–638.

Silva, E., Tsatskis, Y., Gardano, L., Tapon, N., and McNeill, H. (2006). The tumor-suppressor gene fat controls tissue growth upstream of expanded in the hippo signaling pathway. Curr. Biol. *16*, 2081–2089.

Spindle, A.I. (1978). Trophoblast regeneration by inner cell masses isolated from cultured mouse embryos. J. Exp. Zool. *203*, 483–489.

St. John, M.A., Tao, W., Fei, X., Fukumoto, R., Carcangiu, M.L., Brownstein, D.G., Parlow, A.F., McGrath, J., and Xu, T. (1999). Mice deficient of Lats1 develop soft-tissue sarcomas, ovarian tumours and pituitary dysfunction. Nat. Genet. *21*, 182–186.

Strumpf, D., Mao, C.A., Yamanaka, Y., Ralston, A., Chawengsaksophak, K., Beck, F., and Rossant, J. (2005). Cdx2 is required for correct cell fate specification and differentiation of trophectoderm in the mouse blastocyst. Development *132*, 2093–2102.

Tanaka, S., Kunath, T., Hadjantonakis, A.K., Nagy, A., and Rossant, J. (1998). Promotion of trophoblast stem cell proliferation by FGF4. Science *282*, 2072–2075.

Tarkowski, A.K., and Wroblewska, J. (1967). Development of blastomeres of mouse eggs isolated at the 4- and 8-cell stage. J. Embryol. Exp. Morphol. *18*, 155–180.

Thompson, M., Andrade, V.A., Andrade, S.J., Pusl, T., Ortega, J.M., Goes, A.M., and Leite, M.F. (2003). Inhibition of the TEF/TEAD transcription factor activity by nuclear calcium and distinct kinase pathways. Biochem. Biophys. Res. Commun. *301*, 267–274.

Vassilev, A., Kaneko, K.J., Shu, H., Zhao, Y., and DePamphilis, M.L. (2001). TEAD/TEF transcription factors utilize the activation domain of YAP65, a Src/Yes-associated protein localized in the cytoplasm. Genes Dev. *15*, 1229–1241.

Willecke, M., Hamaratoglu, F., Kango-Singh, M., Udan, R., Chen, C.L., Tao, C., Zhang, X., and Halder, G. (2006). The fat cadherin acts through the hippo tumor-suppressor pathway to regulate tissue size. Curr. Biol. *16*, 2090–2100.

Wu, S., Liu, Y., Zheng, Y., Dong, J., and Pan, D. (2008). The TEAD/TEF family protein Scalloped mediates transcriptional output of the Hippo growth-regulatory pathway. Dev. Cell *14*, 388–398.

Yabuta, N., Okada, N., Ito, A., Hosomi, T., Nishihara, S., Sasayama, Y., Fujimori, A., Okuzaki, D., Zhao, H., Ikawa, M., et al. (2007). Lats2 is an essential mitotic regulator required for the coordination of cell division. J. Biol. Chem. *282*, 19259–19271.

Yagi, R., Kohn, M.J., Karavanova, I., Kaneko, K.J., Vullhorst, D., Depamphilis, M.L., and Buonanno, A. (2007). Transcription factor TEAD4 specifies the

trophectoderm lineage at the beginning of mammalian development. Development *134*, 3827–3836.

Yamagata, K., Yamazaki, T., Yamashita, M., Hara, Y., Ogonuki, N., and Ogura, A. (2005). Noninvasive visualization of molecular events in the mammalian zygote. Genesis *43*, 71–79.

Zhang, J., Smolen, G.A., and Haber, D.A. (2008a). Negative regulation of YAP by LATS1 underscores evolutionary conservation of the *Drosophila* Hippo pathway. Cancer Res. *68*, 2789–2794.

Zhang, L., Ren, F., Zhang, Q., Chen, Y., Wang, B., and Jiang, J. (2008b). The TEAD/TEF family of transcription factor Scalloped mediates Hippo signaling in organ size control. Dev. Cell *14*, 377–387.

Zhao, B., Wei, X., Li, W., Udan, R.S., Yang, Q., Kim, J., Xie, J., Ikenoue, T., Yu, J., Li, L., et al. (2007). Inactivation of YAP oncoprotein by the Hippo pathway is involved in cell contact inhibition and tissue growth control. Genes Dev. *21*, 2747–2761.

Zhao, B., Ye, X., Yu, J., Li, L., Li, W., Li, S., Yu, J., Lin, J.D., Wang, C.Y., Chinnaiyan, A.M., et al. (2008). TEAD mediates YAP-dependent gene induction and growth control. Genes Dev. *22*, 1962–1971.

OPEN ACCESS Freely available online

PLoS one

A High-Speed Congenic Strategy Using First-Wave Male Germ Cells

Narumi Ogonuki[1], Kimiko Inoue[1,2], Michiko Hirose[1], Ikuo Miura[1], Keiji Mochida[1], Takahiro Sato[3,5], Nathan Mise[1], Kazuyuki Mekada[1], Atsushi Yoshiki[1], Kuniya Abe[1], Hiroki Kurihara[3], Shigeharu Wakana[1], Atsuo Ogura[1,2,4]*

1 RIKEN BioResource Center, Tsukuba, Ibaraki, Japan, **2** Graduate School of Life and Environmental Science, University of Tsukuba, Tsukuba, Ibaraki, Japan, **3** Department of Physiological Chemistry and Metabolism, Graduate School of Medicine, The University of Tokyo, Bunkyo-ku, Tokyo, Japan, **4** Center for Disease Biology and Integrative Medicine, Graduate School of Medicine, The University of Tokyo, Bunkyo-ku, Tokyo, Japan, **5** Tsukuba Safety Assessment Laboratories, Banyu Pharmaceutical Company Limited, Tsukuba, Ibaraki, Japan

Abstract

Background: In laboratory mice and rats, congenic breeding is essential for analyzing the genes of interest on specific genetic backgrounds and for analyzing quantitative trait loci. However, in theory it takes about 3–4 years to achieve a strain carrying about 99% of the recipient genome at the tenth backcrossing (N10). Even with marker-assisted selection, the so-called 'speed congenic strategy', it takes more than a year at N4 or N5.

Methodology/Principal Findings: Here we describe a new high-speed congenic system using round spermatids retrieved from immature males (22–25 days of age). We applied the technique to three genetically modified strains of mice: transgenic (TG), knockin (KI) and *N*-ethyl-*N*-nitrosourea (ENU)-induced mutants. The donor mice had mixed genetic backgrounds of C57BL/6 (B6):DBA/2 or B6:129 strains. At each generation, males used for backcrossing were selected based on polymorphic marker analysis and their round spermatids were injected into B6 strain oocytes. Backcrossing was repeated until N4 or N5. For the TG and ENU-mutant strains, the N5 generation was achieved on days 188 and 190 and the proportion of B6-homozygous loci was 100% (74 markers) and 97.7% (172/176 markers), respectively. For the KI strain, N4 was achieved on day 151, all the 86 markers being B6-homozygous as early as on day 106 at N3. The carrier males at the final generation were all fertile and propagated the modified genes. Thus, three congenic strains were established through rapid generation turnover between 41 and 44 days.

Conclusions/Significance: This new high-speed breeding strategy enables us to produce congenic strains within about half a year. It should provide the fastest protocol for precise definition of the phenotypic effects of genes of interest on desired genetic backgrounds.

Citation: Ogonuki N, Inoue K, Hirose M, Miura I, Mochida K, et al. (2009) A High-Speed Congenic Strategy Using First-Wave Male Germ Cells. PLoS ONE 4(3): e4943. doi:10.1371/journal.pone.0004943

Editor: Simon Melov, Buck Institute for Age Research, United States of America

Received December 11, 2008; **Accepted** February 19, 2009; **Published** March 31, 2009

Funding: This work was supported by KAKENHI (20062012 [A.O.] and 19300151 [A.O.]). The funders had no role in study design, data collection and analysis, decision to publish, or preparation of the manuscript.

Competing Interests: The authors have declared that no competing interests exist.

* E-mail: ogura@rtc.riken.go.jp

Introduction

For nearly 30 years, the genetic manipulation of laboratory mice has contributed substantially to the development of many fields in medical research and mammalian biology. Remarkably, by genetically altering the mouse genome with single nucleotide precision, it is now possible to create mice with desired genetic modifications to assess gene function in healthy animals and in animal models for human diseases. One major issue associated with mouse genetic engineering is that the biological function of engineered genes can vary with their genetic background [1–3]. This often raises serious concerns, because transgenic (TG) or knockout (or knockin, KI) mice are generated in strains that have historically been selected for the ease and convenience of generating the TG or knockout strain, rather than phenotypic characterization of the mutation itself. For example, most embryonic stem (ES) cell lines used for knockout experiments are derived from the 129 strain. Unfortunately, however, this strain has significant biological limitations that interfere with the phenotypic analysis of a target mutation. It consists of a diverse and complex family of substrains [4] and many of these have an atypical brain structure [5]. Therefore, for facilitating definition of transgene or gene-targeted effects over a given genetic background, the engineered gene should be introduced from the donor strain into the desired recipient strain.

The classical protocol for such purpose is congenic breeding: serially backcrossing the gene donor to the recipient strain accompanied by selection for progeny carrying the desired gene in each backcross generation. This protocol calls for 10 backcross generations (N10), followed by an intercross (F1) to produce founders that are homozygous for the desired gene (theoretically more than 99% of the genome) [6]. Although the strategy is

simple, the process is expensive and time consuming, requiring roughly 3–4 years to produce any given congenic strain. To overcome this weakness, reduction of backcross generations for the establishment of congenic strains has been achieved using marker-assisted selection protocols (MASP), the so-called 'speed congenics'. The time required for deriving such congenic strains is about 1–2 years, depending on the robustness and intensiveness of the polymorphic analysis between the gene donor and recipient strains [7].

One interesting suggestion is that the breeding cycle could be shortened by superovulating and breeding juvenile females (3–4 weeks) followed by embryo transfer to mature females for production of the next generation [8]. This might shorten the generation time down to 6–7 weeks and reduce the whole congenic procedure to 1 year. This 'supersonic congenics' strategy was promising, but has not proved practical because of the limited number of oocytes that can be produced and because there are great individual differences in response to superovulation resumes.

We have attempted to develop another high-speed congenic strategy through the male germline. Recently, we have shown that the genomes of male germ cells from the first wave of spermatogenesis have the ability to support embryonic development to term. Mouse round spermatids—the youngest haploid male germ cells—appear first at 17 days after birth and can be used for the production of offspring by round spermatid injection (ROSI) into oocytes [9]. We applied this technique to the generation of congenic strains from mice with mixed genotypes bearing a transgene, a targeted KI gene or chemically induced mutant genes. At each generation, males used for backcrossing were selected based on polymorphic marker analysis: low density screening MASP using 74–176 markers distributed uniformly throughout the genome. The recipient strain for the expected genetic background was C57BL/6 for all lines of congenics. The results were very consistent and the time for producing a congenic strain was reduced significantly. Therefore, our high-speed congenic system would be very useful for the accelerated analysis of genes of interest under a defined genetic background.

Results and Discussion

Definition of the optimal male age for spermatid collection

In mice, round spermatids can be collected from 17-day-old males at the earliest and their genomes can support full term embryonic development after injection into oocytes using ROSI [9]. However, the efficiency of producing offspring using these round spermatids was extremely low (0.9%) because of their very low incidence in testicular cell suspensions (<2%). This might compromise the accurate identification of round spermatids within a limited time of oocyte micromanipulation. Therefore, we first checked the proportion of round spermatids in testicular cell suspensions from males aged 18, 20, 22 and 24 days to define the optimal age for applying ROSI. As shown in Figure 1, the percentages of round spermatids in testicular suspension increased consistently from days 18 to 24 with statistically significant differences between groups ($P<0.05$). This resulted in easier identification of round spermatids under a microscope: thus, the time required for picking up a single round spermatid was roughly 60, 15, 10 and 10 sec using cell suspensions collected at days 18, 20, 22 and 24, respectively. Therefore, we defined day 22 to be the earliest age of males that allowed the efficient identification of round spermatids in testicular cell suspensions. Testes of the mice at day 22 were smaller than in adults, but we could still collect sufficient round spermatids from a single testis to perform a ROSI experiment (about 150–250 injected oocytes).

Congenics of gene-modified strains using first-wave round spermatids

To test whether high-speed congenics using the first wave of round spermatids could be used practically, we applied the technique to three different types of gene-modified strains, TG, KI and *N*-ethyl-*N*-nitrosourea (ENU)-mutant strains. At each generation, a male used for the next application of ROSI was selected based on showing fewer heterozygous alleles by polymorphic markers that could identify the donor (DBA/2 and 129) and

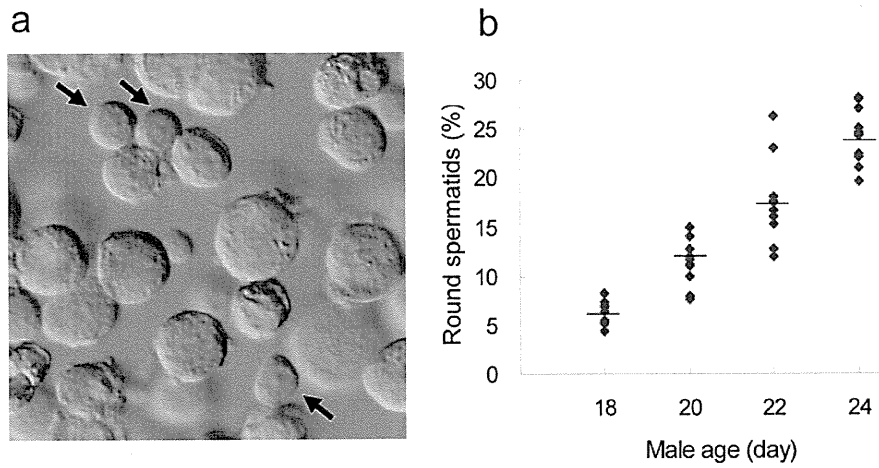

Figure 1. Definition of the optimal male age for spermatid collection. a) Representative photomicrograph of a cell suspension prepared from the testis of a male mouse at 24 days of age. Arrows indicate round spermatids, which are easily identified by a round nucleus and a high cytoplasmic/nuclear ratio. b) The proportion of round spermatids among testicular cells from 18 days to 24 days after birth. The percentages of round spermatids in testicular suspension increased consistently from days 18 to 24 ($P<0.05$ between groups). The cells were counted in two different males by two different operators. The horizontal bars indicate the average.
doi:10.1371/journal.pone.0004943.g001

recipient strains (B6Cr and B6J). Backcross ROSI was repeated until the N4 or N5 generation. After this, additional backcrossing was continued by natural mating to reduce the undetected gaps of contaminating donor alleles [10].

The *Vasa–Venus* TG strain we used was generated from embryos produced by IVF using (B6Cr×DBA/2)F1 strain oocytes and B6Cr strain spermatozoa, and maintained by full-sib mating. The N1 offspring were obtained by ICSI using a donor male at F7. As shown in Figure 2a, N5 backcross offspring were obtained on day 188 and all 74 markers were identified as B6 homozygous in one of two carrier males.

The *Ednra*$^{EGFP/+}$ KI strain was derived from ES cells with a (B6Cr×129^{+Ter}/SvJcl)F1 genetic background [11]. The first N1 generation was obtained by IVF using B6Cr oocytes and spermatozoa from a chimeric mouse. All 86 markers were homozygous for B6Cr as early as at N3 (day 106; 2 out of 14 carrier males) and N4 offspring were obtained on day 151 (Figure 2b).

The ENU-induced growth differentiation factor 5 (*Gdf5*) mutant line had a mixed genetic background of B6J and DBA/2J [12]. For this combination of inbred strains, more dense polymorphic markers were available using single nucleotide polymorphism (SNP) assays as well as microsatellite genotyping (176 markers; see Materials and Methods). The N5 generation was obtained on day 190 and was 97.7% (172/176) homozygous for B6J (Figure 2c). The following N6 and N7 generations produced by IVF were 98.8% and 99.4% homozygous for B6J, respectively.

The efficiency rates in backcross breeding by ROSI in these gene-modified strains are shown in Table 1. All the modified genes could be propagated successfully into the next generations by ROSI. The male carriers finally obtained were all fertile and propagated the modified genes to the next generation by natural mating.

Significance of congenic breeding using first-wave male germ cells

Congenic strains have been used extensively for the study of mouse genetics including definition of phenotypic effects of genes on specific genetic backgrounds and identification of genes or genomic segments affecting the phenotypes of interest by quantitative trait locus (QTL) analysis. However, it takes about 2–3 years to construct a congenic strain with a level of genetic homogeneity that is reliable for research (>99% or more) [6]. To accelerate congenic breeding, MASP has been developed by taking advantage of precise information on mouse genetics [7]. Another approach for efficient congenics should be rapid generation turnover by assisted reproduction techniques. The use of immature females proposed by Behringer [8] was applied

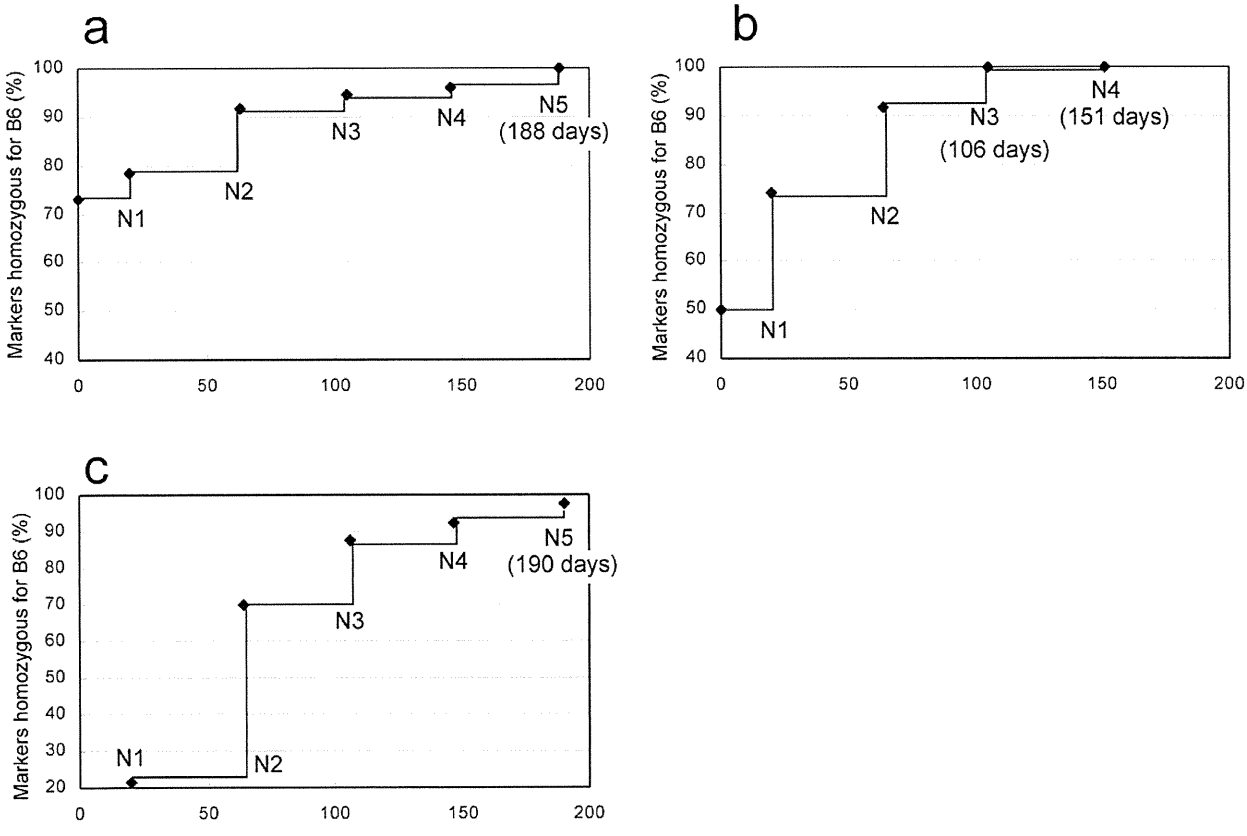

Figure 2. Time course of generation turnover and the rate of markers homozygous for the C57BL/6 (B6) type. a) *Vasa–Venus* transgenic strain. All markers (n = 74) were homozygous for B6 at N5 on day 188. b) *Ednra*$^{EGFP/+}$ knockin strain. All markers (n = 86) were homozygous for B6 at N3 on day 106 and N4 offspring were obtained on day 151. c) ENU-induced *Gdf5* mutant strain. The N5 generation was obtained on day 190 and was 97.7% (172/176) homozygous for B6. There were 74, 86 and 176 polymorphic markers, which identified the alleles for the C57BL/6Cr:DBA/2Cr, C57BL/6Cr:129 and C57BL/6J:DBA/2J strains, respectively. Each generation turnover was between 42 and 45 days: the age of the donor male plus the gestation period (20 days) minus the one-day overlap between them.
doi:10.1371/journal.pone.0004943.g002

Table 1. Results of congenic breeding by round spermatid injection (ROSI) in three gene-modified strains.

Strain	Generation produced	Age (day) of male used for ROSI	No. of oocyes that survived ROSI	No. (%) of oocytes that developed to 2-cells	No. of 2-cells transferred	No. (%) implanted	No. (%) born	No. (%) of males born	No. (%) of male carriers
Vasa-Venus transgenic	N1	Adult (ICSI)	16	15 (93.8)	15	10 (66.7)	5 (33.3)	5 (33.3)	5 (33.3)*
	N2	24	182	164 (90.1)	164	69 (42.1)	24 (14.6)	12 (7.3)	4 (2.4)
	N3	23	123	109 (88.6)	109	24 (22.0)	4 (3.7)	2 (1.8)	1 (0.9)
	N4	22	172	156 (90.7)	156	51 (32.7)	14 (9.0)	6 (3.8)	2 (1.3)
	N5	23	134	123 (91.8)	123	23 (18.7)	10 (8.1)	4 (3.3)	2 (1.6)
Ednra-EGFP knockin**	N1	Adult (IVF)	166	135 (81.3)	135	62 (45.9)	49 (36.3)	23 (17.0)	12 (8.9)
	N2	24	243	196 (80.7)	196	63 (32.1)	30 (15.3)	10 (5.1)	5 (2.6)
	N3	24	261	235 (90.0)	235	107 (45.5)	52 (22.1)	30 (12.8)	14 (6.0)
	N4	25	244	215 (88.1)	215	72 (33.5)	39 (18.1)	19 (8.8)	11 (5.1)
ENU-induced mutant	N1	Adult (IVF)	80	49 (61.3)	49	Not observed	26 (53.1)	14 (28.6)	3 (6.1)
	N2	25	201	158 (78.6)	158	54 (34.2)	25 (15.8)	11 (7.0)	4 (2.5)
	N3	23	208	194 (93.3)	194	68 (35.1)	26 (13.4)	12 (6.2)	7 (3.6)
	N4	22	173	127 (73.4)	127	51 (40.2)	13 (10.2)	5 (3.9)	2 (1.6)
	N5	24	216	177 (81.9)	177	91 (51.4)	34 (19.2)	10 (5.6)	4 (2.3)
Total (ROSI only)			2157	1854 (86.0)	1854	673 (36.3)	271 (14.6)	121 (6.5)	56 (3.0)
Control (C57BL/6)		22–24	467	349 (74.7)	329	133 (40.4)	49 (14.9)	26 (7.9)	

*The implantation sites were identified as the scars of decidualization at caesarian section.
**The donor male (N0) was homozygous for the transgene.
***All genetic markers tested were homozygous for the B6 mouse strain at N3.
doi:10.1371/journal.pone.0004943.t001

successfully to the derivation of a conplastic strain of rats [13]. However, there have been very few similar applications published, probably because of the limited number of oocytes produced from any one female, which may attenuate the number of carrier females in the subsequent generations. Our high-speed congenic system uses immature males as founders at each generation. Unlike females, each male can produce a large number of germ cells and multiple litters of offspring. This not only assures the safe propagation of the target gene on to the next generation, but also enables efficient selection of a male for the next round of ROSI, thus significantly shortening the time for congenics.

In this study, the advantages of our high-speed congenic strategy were shown in the KI strain, which started with a (B6Cr×129)F1 genetic background: all 86 markers were homozygous for the B6 strain as early as 106 days (N3). Apparently, it is more straightforward to use B6 ES cells for gene targeting if the B6 genetic background is required. Several B6 ES cells are available for gene targeting [14,15], and the International Knockout Consortium uses C57BL/6 ES cell lines [16]. However, B6 ES cells usually require more intense care than other 129 or hybrid ES cells to maintain their germline transmission ability during gene targeting. ES cells with hybrid genetic constitutions of B6 and 129 are easy to maintain and can be used efficiently for producing gene-targeted offspring [1,11], especially by tetraploid complementation [17]. If the gene-targeted allele is of B6 origin, it may avoid the persistence of donor genetic segments around the targeted allele during congenic production, which inevitably occurs when 129 ES cells are used. Thus, the combination of gene-targeting (B6×129)F1 ES cells and the new high-speed congenic breeding may be an alternative fast protocol to generate a B6 gene-targeting strain.

A congenic breeding strategy has also been employed extensively in laboratory rats because it is now possible to map the genetic variants and mutations that underlie complex disease-related phenotypes in this species [18,19]. ROSI is successful in some, but not all, strains of rats [20]. As the first wave of round spermatids appears in rat testes around 26 days after birth, we estimate that congenic rat strains could be generated within 7 or 8 months by using these germ cells [21].

We anticipate that the congenic strategy developed in this study might be accelerated further using male germ cells that are younger than round spermatids. This is possible theoretically, because the genomes of primary spermatocytes—premeiotic male germ cells—can support the full term development of embryos [22]. Despite many efforts to improve the technique, however, the efficiency of producing offspring using primary spermatocytes is very low [22,23]. Therefore, at present the use of round spermatids on days 22–25 may be the most practical range for efficient, rapid backcross breeding in mice. As far as we know, this is the most rapid generational turnover by sexual reproduction in mammals.

Technical issues associated with congenics by ROSI

As mentioned above, the high-speed congenic strategy we developed is very promising to produce congenic strains with desired genetic backgrounds. One of the technical issues associated with this strategy is that ROSI needs some skill and experience. However, ROSI is generally easier to perform than conventional ICSI because of the high survival rate of oocytes after injection: the diameter of injection pipettes is small and the activated oocytes used for ROSI are more resistant to the injection stimulus than nonactivated oocytes [24]. From our experience, training of three

to four consecutive weeks is enough for ROSI if the operator already has the basic technique for embryo handling. For ICSI, reliable protocol papers are available [25,26] and the same protocols can be essentially applied to ROSI. Oocytes from B6 females tend to be more sensitive to injection than those from other strains, but this problem might be overcome by using a high osmotic strength medium for manipulation on the microscope stage, if necessary. In our ROSI experiments using B6 oocytes, about 80% survived the injection whereas about 90% survived in other strains including B6D2F1, DBA/2 and 129 (unpublished).

As shown in Table 1, we consistently obtained sufficient carrier males for selection except for the N3 to N5 generations in the *Vasa–Venus* TG strain, which were affected by an accidental decline in the quality of recipient females, for reasons unknown. Based on the overall efficiency in our ROSI experiments presented in Table 1, we estimated the number of oocytes to be injected with the aim of obtaining expected number of carrier males (Table 2). These numbers of oocytes can be handled by one or two operators in a single session.

One can question if epigenetic modifications might have occurred during conception using round spermatids, because ROSI-derived preimplantation embryos have shown some disturbances in gene expression [27,28] and aberrant DNA methylation [29]. However, epigenetic errors imposed on individuals are normally erased during germ cell development and are never transmitted to the next generation by natural mating, as shown in mouse somatic cell cloning experiments [30,31]. Therefore, once mated naturally, congenic strains produced by ROSI are expected to become epigenetically indistinguishable from those produced by conventional congenic protocols.

Conclusions

The generation turnover time in mice can be shortened to about 40 days by using the first wave round spermatids as male gametes. We confirmed that this breeding strategy reduced the time required for congenesis to about half a year. This should provide the earliest opportunities for the analysis of genes of interest under a defined genetic background and for QTL mapping, which are becoming integral to biomedical research using the mouse as a model.

Materials and Methods

The origin of donor strains

The B6 substrains used in this study were B6Cr (C57BL/6CrSlc) and B6J (C57BL/6JJcl), which were purchased from CLEA Japan, Inc. (Kanagawa) and Japan SLC, Inc. (Shizuoka), respectively [32]. One mature male mouse from each strain was used as the donor of the modified gene. The TG strain we used was Tg(Mvh-Venus)1Rbrc, which was generated by DNA nuclear injection into zygotes derived from IVF using (B6Cr×DBA/2)F1 oocytes and B6Cr spermatozoa. The *Mvh-Venus* gene clearly shows the germline origin of living cells by green fluorescence because of the highly specific expression of the *Mvh* (mouse vasa homologue) gene [33]. The strain was maintained by full-sib mating. An F7 male homozygous for the transgene was used as the donor.

The KI line we used was the $Ednra^{EGFP/+}$ strain carrying the reporter gene for enhanced green fluorescence protein (EGFP) that had been knocked into the *Ednra* (endothelin receptor type A) locus by recombinase-mediated cassette exchange based on the Cre-lox system [11]. The gene-targeted ES cells had the (B6Cr×129^{+Ter}/SvJcl)F1 genotype. Chimeric embryos were produced by injection of ES cells into ICR blastocysts and they were transferred into pseudopregnant ICR females. A chimeric male thus obtained were used for producing N1 by conventional IVF using B6Cr oocytes.

The ENU-induced mutant strain we used carried a point mutation at the *Gdf5* locus. This mutation causes an amino acid substitution in a highly conserved region of the active signaling domain of the GDF5 (growth differentiation factor 5) protein, leading to impaired joint formation and osteoarthritis [12]. The donor male had a mixed genetic background of B6J and DBA/2 because the strain was generated from a cross of an ENU-mutagenized B6J male and a wild-type DBA/2 female.

Offspring that carried modified genes were genotyped at each generation by polymerase chain reaction (PCR) amplification with specific primers for the given TG strain [34], by specific green fluorescence over the body for the KI strain and by PCR-based sequencing for the ENU mutant strain [12].

Table 2. The numbers of superovulated females and oocytes required for obtaining selectable numbers of carrier males, as estimated from the data in Table 1.

Females superovulated (25–30 oocytes per female)	4 to 5	6 to 7	7 to 8
Oocytes injected	125	167	208
Oocytes survived (80% per oocytes injected)	100	133	167
2-cells transferred (80% per oocytes survived)	80	107	133
Birth (15% per 2-cells transferred)	12	16	20
Males (50% per birth)	6	8	10
Carrier males (50% per males)	3	4	5

doi:10.1371/journal.pone.0004943.t002

Collection of oocytes

Female B6Cr or B6J strain mice (7–10 weeks old) were each injected with 7.5 units of equine chorionic gonadotropin followed by injection of 7.5 units of human chorionic gonadotropin (hCG) 48 h later. Mature oocytes were collected from the oviducts 15–17 h after hCG injection and were freed from cumulus cells by treatment with 0.1% hyaluronidase in CZB medium [35]. The oocytes were transferred to fresh CZB medium and incubated at 37°C in an atmosphere of 5% CO_2 in air for up to 90 min before ROSI.

Preparation of testicular cell suspensions

Spermatogenic cells were prepared mechanically as described for hamsters [36]. Briefly, testes were removed from 18- to 25-day-old males and placed in erythrocyte-lysing buffer (155 mM NH_4Cl/10 mM $KHCO_3$/2 mM EDTA, pH 7.2). For the first series of experiments to identify the optimal age of males for donors, we used ICR males; as far as we examined there were no strain-dependent differences in the timing of the first wave of spermatogenesis. The tunica albuginea was removed and the seminiferous tubule masses were transferred into cold (4°C) Dulbecco's phosphate buffered saline (PBS) supplemented with 5.6 mM glucose, 5.4 mM sodium lactate and 0.1 mg/ml of polyvinyl alcohol (polyvinylpyrrolidone, PVP, in the original report) (GL-PBS) [36]. The seminiferous tubules were cut into small pieces and pipetted gently to disperse spermatogenic cells into the GL-PBS. Then, the cell suspension was filtered through a 38-μm nylon mesh and washed three times by centrifugation (200 *g* for 4 min). To define the optimal male age for spermatid collection, we first examined the proportion of round spermatids in

cell suspensions collected from two males aged at 18, 20, 22, or 24 days. The percentages of round spermatids were analyzed using arcsine transformation, followed by one-way ANOVA analysis and a *post-hoc* procedure using Scheffe's test for multiple comparisons.

ROSI

ROSI was performed using a Piezo-driven micromanipulator (Prime Tech Ltd., Ibaraki, Japan) as described [37,38]. The cover of a plastic dish (Falcon no. 1006; Becton Dickinson, Franklin Lakes, NJ) was used as a microinjection chamber. Several small drops (~4 μl) of Hepes-buffered CZB with or without 10% PVP were placed on the bottom and covered with mineral oil. Spermatogenic cells were placed in one of the PVP droplets. Before injection of the nuclei of round spermatids, oocytes were activated by treatment with Ca^{2+}-free CZB medium containing 2.5 mM $SrCl_2$ for 20 min at 37°C. Oocytes reaching telophase II at 40–90 min after onset of activation treatment were each injected with a round spermatid. They were kept in Hepes-CZB at room temperature (24°C) for ~10 min before culture in CZB at 37°C under 5% CO_2 in air.

Embryo culture and transfer

Embryos that reached the 2-cell stage by 24 h of culture in CZB were transferred into the oviducts of pseudopregnant ICR strain females (8–12 weeks old) on the day after mating (day 0.5). On day 19.5, recipient females were killed and their uteri were examined for live term fetuses. These were nursed by lactating ICR foster females. The day of birth was designated day 0.5 for newborns.

Care and use of animals

All procedures described here were reviewed and approved by the Animal Experimental Committee at the RIKEN Institute.

Genotyping for MASP

Tail clips about 0.3 cm long were collected for DNA extraction, using the Wizard Genomic DNA Purification Kit (Promega, Madison, WI) and the DNeasy 96 Blood & Tissue Kit (#69582; QIAGEN GmbH, Hilden, Germany) according to the manufacturers' instructions. Microsatellite genotyping was carried out by PCR for simple sequence length polymorphisms (SSLP) using microsatellite markers. The microsatellite markers were selected out of sequence length polymorphisms between B6 and DBA/2 and B6 and 129 strains (Mekada et al., unpublished data) (Tables S1 and S2). PCR execution was performed using the QIAGEN Multiplex PCR kit (#206143; QIAGEN GmbH) and the length polymorphism was detected by agarose gel electrophoresis. Map locations and primer sequences of the microsatellite loci were used according to the Mouse Genome Informatics (MGI) of the Jackson Laboratory, USA, and Mouse Microsatellite Data Base of Japan (MMDBJ).

SNP genotyping was carried out using a TaqMan Minor Groove Binding (MGB) assay (Applied Biosystems, Foster City, CA). TaqMan MGB probe sets were designed based on SNP polymorphism between C57BL/6J and DBA/2J (Table S3). PCR execution was performed using TaqMan Genotyping Master Mix (#4371353; Applied Biosystems). SNP polymorphisms were detected using an ABI PRISM 7900HT Sequence Detection System (Applied Biosystems).

Supporting Information

Table S1 Variation alleles between C57BL/6 and DBA/2 mouse strains.
Found at: doi:10.1371/journal.pone.0004943.s001 (0.02 MB XLS)

Table S2 Variation alleles between C57BL/6 and 129 mouse strains.
Found at: doi:10.1371/journal.pone.0004943.s002 (0.02 MB XLS)

Table S3 The SNPs information that designed the TaqMan MGB probe sets.
Found at: doi:10.1371/journal.pone.0004943.s003 (0.02 MB XLS)

Acknowledgments

We would like to thank Drs. Masumi Hirabayashi and Hiromi Miki for discussion on round spermatid injection techniques and Dr. Tomokazu Amano for the genetic information on the (B6×129)F1 ES cell line.

Author Contributions

Conceived and designed the experiments: NO AO. Performed the experiments: NO KI MH IM KM KM. Analyzed the data: NO IM SW AO. Contributed reagents/materials/analysis tools: TS NM KM AY KA YK. Wrote the paper: NO IM SW AO.

References

1. Glaser S, Anastassiadis K, Stewart AF (2005) Current issues in mouse genome engineering. Nat Genet 37: 1187–1193.
2. Yoshiki A, Moriwaki K (2006) Mouse phenome research: implications of genetic background. ILAR J 47: 94–102.
3. Eisener Dorman AF, Lawrence DA, Bolivar VJ (2008) Cautionary insights on knockout mouse studies: The gene or not the gene? Brain Behav Immun, In press.
4. Simpson EM, Linder CC, Sargent EE, Davisson MT, Mobraaten LE, et al. (1997) Genetic variation among 129 substrains and its importance for targeted mutagenesis in mice. Nat Genet 16: 19–27.
5. Livy DJ, Wahlsten D (1991) Tests of genetic allelism between four inbred mouse strains with absent corpus callosum. J Hered 82: 459–464.
6. Flaherty L (1981) Congenic strains. In: Foster HL, Small JD, Fox JG, eds. The Mouse in Biomedical Research (Vol. 1). New York: Academic Press. pp 215–222.
7. Markel P, Shu P, Ebeling C, Carlson GA, Nagle DL, et al. (1997) Theoretical and empirical issues for marker-assisted breeding of congenic mouse strains. Nat Genet 17: 280–284.
8. Behringer R (1998) Supersonic congenics? Nat Genet 18: 108.
9. Miki H, Lee J, Inoue K, Ogonuki N, Noguchi Y, et al. (2004) Microinsemination with first-wave round spermatids from immature male mice. J Reprod Dev 50: 131–137.
10. Armstrong NJ, Brodnicki TC, Speed TP (2006) Mind the gap: analysis of marker-assisted breeding strategies for inbred mouse strains. Mamm Genome 17: 273–287.
11. Sato T, Kawamura Y, Asai R, Amano T, Uchijima Y, et al. (2008) Recombinase-mediated cassette exchange reveals the selective use of Gq/G11-dependent and -independent endothelin 1/endothelin type A receptor signaling in pharyngeal arch development. Development 135: 755–765.
12. Masuya H, Nishida K, Furuichi T, Toki H, Nishimura G, et al. (2007) A novel dominant-negative mutation in Gdf5 generated by ENU mutagenesis impairs joint formation and causes osteoarthritis in mice. Hum Mol Genet 16: 2366–2375.
13. Pravenec M, Hyakukoku M, Houstek J, Zidek V, Landa V, et al. (2007) Direct linkage of mitochondrial genome variation to risk factors for type 2 diabetes in conplastic strains. Genome Res 17: 1319–1326.
14. Seong E, Saunders TL, Stewart CL, Burmeister M (2004) To knockout in 129 or in C57BL/6: that is the question. Trends Genet 20: 59–62.
15. Pacholczyk G, Suhag R, Mazurek M, Dederscheck SM, Koni PA (2008) Generation of C57BL/6 knockout mice using C3H×BALB/c blastocysts. Biotechniques 44: 413–416.
16. Collins FS, Rossant J, Wurst W (2007) A mouse for all reasons. Cell 128: 9–13.
17. George SH, Gertsenstein M, Vintersten K, Korets Smith E, Murphy J, Stevens ME, Haigh JJ, Nagy A (2007) Developmental and adult phenotyping

directly from mutant embryonic stem cells. Proc Natl Acad Sci U S A 104: 4455–4460.
18. Aitman TJ, Critser JK, Cuppen E, Dominiczak A, Fernandez-Suarez XM, et al. (2008) Progress and prospects in rat genetics: a community view. Nat Genet 40: 516–522.
19. Saar K, Beck A, Bihoreau MT, Birney E, Brocklebank D, et al. (2008) SNP and haplotype mapping for genetic analysis in the rat. Nat Genet 40: 560–566.
20. Hirabayashi M, Kato M, Aoto T, Ueda M, Hochi S (2002) Rescue of infertile transgenic rat lines by intracytoplasmic injection of cryopreserved round spermatids. Mol Reprod Dev 62: 295–299.
21. Jahnukainen K, Chrysis D, Hou M, Parvinen M, Eksborg S, et al. (2004) Increased apoptosis occurring during the first wave of spermatogenesis is stage-specific and primarily affects midpachytene spermatocytes in the rat testis. Biol Reprod 70: 290–296.
22. Ogura A, Suzuki O, Tanemura K, Mochida K, Kobayashi Y, et al. (1998) Development of normal mice from metaphase I oocytes fertilized with primary spermatocytes. Proc Natl Acad Sci U S A 95: 5611–5615.
23. Miki H, Ogonuki N, Inoue K, Baba T, Ogura A (2006) Improvement of cumulus-free oocyte maturation in vitro and its application to microinsemination with primary spermatocytes in mice. J Reprod Dev 52: 239–248.
24. Miki H, Hirose M, Ogonuki N, Inoue K, Kezuka F, et al. Efficient production of androgenetic embryos by round spermatid injection. Genesis, In press.
25. Nagy A, Gertsenstein M, Vintersten K, Behringer R (2003) Manipulating the Mouse Embryo: A Laboratory Manual (3rd edition). New York: Cold Spring Harbor Laboratory Press. 565 p.
26. Yoshida N, Perry AC (2007) Piezo-actuated mouse intracytoplasmic sperm injection (ICSI). Nat Protoc 2: 296–304.
27. Hayashi S, Yang J, Christenson L, Yanagimachi R, Hecht NB (2003) Mouse preimplantation embryos developed from oocytes injected with round spermatids or spermatozoa have similar but distinct patterns of early messenger RNA expression. Biol Reprod 69: 1170–1176.
28. Ziyyat A, Lefevre A (2001) Differential gene expression in pre-implantation embryos from mouse oocytes injected with round spermatids or spermatozoa. Hum Reprod 16: 1449–1456.
29. Kishigami S, Van Thuan N, Hikichi T, Ohta H, Wakayama S, et al. (2006) Epigenetic abnormalities of the mouse paternal zygotic genome associated with microinsemination of round spermatids. Dev Biol 289: 195–205.
30. Shimozawa N, Ono Y, Kimoto S, Hioki K, Araki Y, et al. (2002) Abnormalities in cloned mice are not transmitted to the progeny. Genesis 34: 203–207.
31. Tamashiro KLK, Wakayama T, Akutsu H, Yamazaki Y, Lachey JL, et al. (2002) Cloned mice have an obese phenotype not transmitted to their offspring. Nat Med 8: 262–267.
32. Mekada K, Abe K, Murakami A, Nakamura S, Nakata H, Moriwaki K, Obata Y, Yoshiki A (2009) Genetic differences among C57BL/6 substrains. Exp Anim, In press.
33. Fujiwara Y, Komiya T, Kawabata H, Sato M, Fujimoto H, et al. (1994) Isolation of a DEAD-family protein gene that encodes a murine homolog of Drosophila vasa and its specific expression in germ cell lineage. Proc Natl Acad Sci U S A 91: 12258–12262.
34. Nagai T, Ibata K, Park ES, Kubota M, Mikoshiba K, et al. (2002) A variant of yellow fluorescent protein with fast and efficient maturation for cell-biological applications. Nat Biotechnol 20: 87–90.
35. Chatot CL, Ziomek CA, Bavister BD, Lewis JL, Torres I (1989) An improved culture medium supports development of random-bred 1-cell mouse embryos in vitro. J Reprod Fertil 86: 679–688.
36. Ogura A, Yanagimachi R (1993) Round spermatid nuclei injected into hamster oocytes form pronuclei and participate in syngamy. Biol Reprod 48: 219–225.
37. Kimura Y, Yanagimachi R (1995) Mouse oocytes injected with testicular spermatozoa or round spermatids can develop into normal offspring. Development 121: 2397–2405.
38. Ogonuki N, Mochida K, Miki H, Inoue K, Fray M, et al. (2006) Spermatozoa and spermatids retrieved from frozen reproductive organs or frozen whole bodies of male mice can produce normal offspring. Proc Natl Acad Sci U S A 103: 13098–13103.

Sirt3 protects in vitro–fertilized mouse preimplantation embryos against oxidative stress–induced p53-mediated developmental arrest

Yumiko Kawamura,[1] Yasunobu Uchijima,[1] Nanao Horike,[1] Kazuo Tonami,[1] Koichi Nishiyama,[1] Tomokazu Amano,[1] Tomoichiro Asano,[2] Yukiko Kurihara,[1] and Hiroki Kurihara[1]

[1]Department of Physiological Chemistry and Metabolism, Graduate School of Medicine, University of Tokyo, Tokyo, Japan.
[2]Department of Biomedical Chemistry, Hiroshima University Graduate School of Biomedical Sciences, Hiroshima, Japan.

Sirtuins are a phylogenetically conserved NAD^+-dependent protein deacetylase/ADP-ribosyltransferase family implicated in diverse biological processes. Several family members localize to mitochondria, the function of which is thought to determine the developmental potential of preimplantation embryos. We have therefore characterized the role of sirtuins in mouse preimplantation development under in vitro culture conditions. All sirtuin members were expressed in eggs, and their expression gradually decreased until the blastocyst stage. Treatment with sirtuin inhibitors resulted in increased intracellular ROS levels and decreased blastocyst formation. These effects were recapitulated by siRNA-induced knockdown of Sirt3, which is involved in mitochondrial energy metabolism, and in *Sirt3*$^{-/-}$ embryos. The antioxidant *N*-acetyl-*L*-cysteine and low-oxygen conditions rescued these adverse effects. When Sirt3-knockdown embryos were transferred to pseudopregnant mice after long-term culture, implantation and fetal growth rates were decreased, indicating that Sirt3-knockdown embryos were sensitive to in vitro conditions and that the effect was long lasting. Further experiments revealed that maternally derived Sirt3 was critical. Sirt3 inactivation increased mitochondrial ROS production, leading to p53 upregulation and changes in downstream gene expression. The inactivation of p53 improved the developmental outcome of Sirt3-knockdown embryos, indicating that the ROS-p53 pathway was responsible for the developmental defects. These results indicate that Sirt3 plays a protective role in preimplantation embryos against stress conditions during in vitro fertilization and culture.

Introduction

Infertility, defined as failure to conceive after 2 years of unprotected intercourse, is a major social and personal problem affecting approximately 10% of couples worldwide. Assisted reproductive technologies, such as in vitro fertilization (IVF), are widely used for the treatment of infertility in clinical practice, but many issues impeding therapeutic efficacy remain to be solved (1–3). In general, human reproduction is inefficient, with more than 60% of fertilized embryos unable to survive to delivery, mainly because of early developmental failure before and during implantation (4, 5). Although various intrinsic and environmental factors have been proposed to affect early embryogenesis, the mechanisms determining developmental potential remain largely unveiled.

It has recently been postulated that mitochondrial function is a possible determinant of developmental potential in preimplantation embryos (6, 7). Although mitochondria within eggs and preimplantation embryos are morphologically premature and their oxygen consumption is relatively low, blockade of oxidative phosphorylation and perturbation of mitochondrial membrane integrity exerts a detrimental effect on preimplantation development (8–10). Furthermore, ATP content within individual eggs is correlated with reduced developmental competence and postimplantation outcomes (11). In addition to ATP synthesis through oxidative phosphorylation, mitochondria play diverse roles in signal transduction, calcium homeostasis, and oxygen metabolism. In particular, ROS generated in mitochondrial electron transport chain, together with cytoplasmic NAD(P)H oxidase and xanthine oxidase, has been implicated in various biological processes (12–14). Oxidative stress caused by excessive production of ROS and/or impaired antioxidant defense mechanisms has been shown to be detrimental to germ cells and fertilized eggs, resulting in the impairment of early embryonic development (15–17). Involvement of mitochondrial dysfunction in this process has also been reported (18).

Recently, the sirtuins, deacetylase/ADP-ribosyltransferase proteins with homology to the yeast silent information regulator 2 (Sir2), have emerged as a key mediator between energy metabolism and cellular signaling in various species (19–21). The lysine deacetylation activity of sirtuins is characteristically upregulated by NAD^+ and downregulated by NADH and nicotinamide, a product of the deacetylation reaction; sirtuins are thereby postulated to link the cellular energy state to biochemical signals by sensing NAD^+/NADH levels (22, 23). In mammals, 7 proteins (Sirt1–Sirt7) are known to constitute the sirtuin family and are implicated in many physiological events, such as aging, cell metabolism, apoptosis, and cell cycle regulation (19–21). Among the sirtuin members, Sirt3, Sirt4, and Sirt5 are characterized by their localization to the mitochondria (24–27). Previous studies have revealed that Sirt3 is involved in the regulation of mitochondrial proteins such as acetyl-CoA synthase 2 (AceCS2) through its deacetylation activity (28, 29).

Conflict of interest: The authors have declared that no conflict of interest exists.
Citation for this article: *J Clin Invest.* 2010;120(8):2817–2828. doi:10.1172/JCI42020.

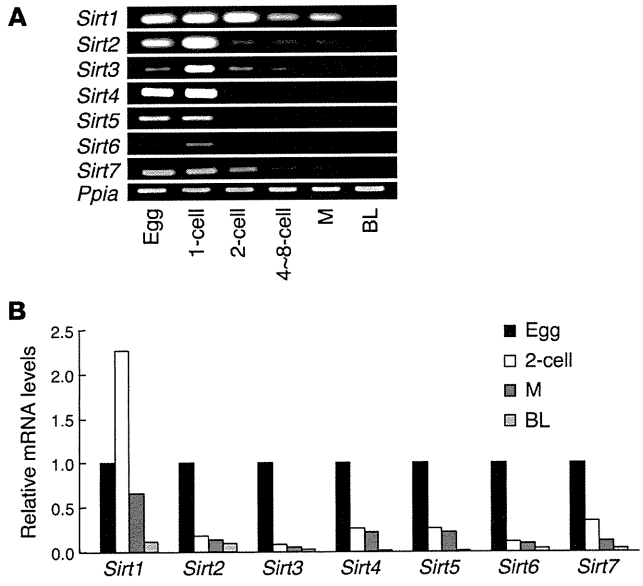

Figure 1
Sirtuin gene expression in mouse eggs and preimplantation embryos. (**A**) Conventional RT-PCR analysis. Eggs and preimplantation embryos were collected for RNA sampling from the oviducts or uteri at the appropriate time for each stage as follows: egg, 1-cell, 2-cell, approximately 4- to 8-cell, morula (M), and blastocyst (BL). *Ppia* expression served as an internal control. (**B**) Relative quantification of sirtuin mRNA levels by real-time RT-PCR.

In addition, gene-knockout experiments have elucidated the role of Sirt3 in the regulation of mitochondrial activity and basal ATP synthesis (30). However, *Sirt3*$^{-/-}$ mice demonstrate no obvious phenotype in spite of a 50% reduction in ATP levels, which indicates that the basal metabolic state could stand this reduction, but phenotype might become apparent under certain stress conditions (30, 31).

In the present study, we investigated whether sirtuin might serve as a contributing factor to the developmental potential of preimplantation embryos. We demonstrated that Sirt3 played a protective role in mouse preimplantation embryos under in vitro culture conditions. Whereas *Sirt3*$^{-/-}$ mice were fertile, IVF and in vitro–cultured *Sirt3*$^{-/-}$ or Sirt3 siRNA–induced knockdown embryos were susceptible to developmental defects. Our results further indicated the involvement of tumor suppressor p53 induction, possibly triggered by mitochondrial ROS, in Sirt3 deficiency–induced developmental arrest. These findings may implicate Sirt3 activity in successful IVF outcome as a regulator of mitochondrial function.

Results

Sirtuins are expressed in mouse eggs and preimplantation embryos. To investigate the possible involvement of sirtuins in preimplantation development, we first examined the expression of *Sirt1*–*Sirt7* genes in eggs and early embryos using specific primers (Supplemental Table 1; supplemental material available online with this article; doi:10.1172/JCI42020DS1). In eggs and early embryos, expression of all the sirtuin members was detected by RT-PCR (Figure 1). After the first cleavage, *Sirt1*–*Sirt7* expression was downregulated with distinct time courses (Figure 1).

Sirtuin inhibitors cause developmental defects and increased mitochondrial ROS generation in preimplantation embryos. We next examined whether blockade of sirtuin activities affects preimplantation development. Nicotinamide, a product of the sirtuin deacetylation reaction and an inhibitor of sirtuin activity, has been reported to suppress blastocyst formation and subsequent postimplantation development (32). Consistently, nicotinamide, but not nicotinic acid, inhibited preimplantation development after IVF (Figure 2A) as early as the second cleavage stage (Supplemental Figure 1). In addition, 2 other sirtuin deacetylase inhibitors, sirtinol and N-(2-aminophenyl)-N′-phenyloctanediamide (BML-210), also inhibited development after IVF, with stage profiles similar to that of nicotinamide treatment (Figure 2B and Supplemental Figure 2).

In another series of experiments, we detected an increase in the fluorescence intensity emitted by 5-(and-6)-chloromethyl-2′,7′-dichlorodihydrofluorescein diacetate (CM-H_2DCFDA) fluorescent dye in sirtinol-treated embryos. This increase in fluorescent signals was abolished by treatment with the antioxidant *N*-acetyl-*L*-cysteine (NAC; Figure 2, C and E) and the mitochondrial complex III inhibitor stigmatellin (Figure 2, D and F), which also inhibits complex I at higher concentrations (33). Our observations indicate that intracellular ROS levels were increased by sirtinol, and excessive ROS generation by mitochondria appeared to be responsible for this phenomenon. These findings suggest the possible involvement of sirtuin activity in normal progression of preimplantation development and control of intracellular ROS levels.

Sirtuins are upregulated by oxidative stress. During fertilization and preimplantation development in vitro, oxidative stress imposed by excessive intracellular ROS levels is supposed to cause a harmful effect on gametes and embryos (15–17). Therefore, we speculated that the expression of sirtuins might be upregulated by oxidative stress to provide protective feedback in early embryos. To test this possibility, we incubated 4-cell embryos with media containing H_2O_2 and examined changes in sirtuin mRNA levels by RT-PCR. Exposure to 20 μM H_2O_2 for 6 hours resulted in increased *Sirt3* expression in embryos (Figure 3A). H_2O_2-induced increases in Sirt3 protein levels were confirmed in embryos at the same stage (Figure 3B) and in NIH 3T3 cells (Figure 3C). Because Sirt3 is a mitochondrial deacetylase involved in the regulation of mitochondrial electron transport, and because mitochondria are the major source of ROS and a determinant of developmental competence of preimplantation embryos (6, 9, 34), we therefore focused on Sirt3 in subsequent experiments.

Sirt3 is localized to mitochondria in eggs and preimplantation embryos. Sirt3 has been described as a mitochondrial sirtuin, but recent studies have reported that it is also localized to the nucleus in

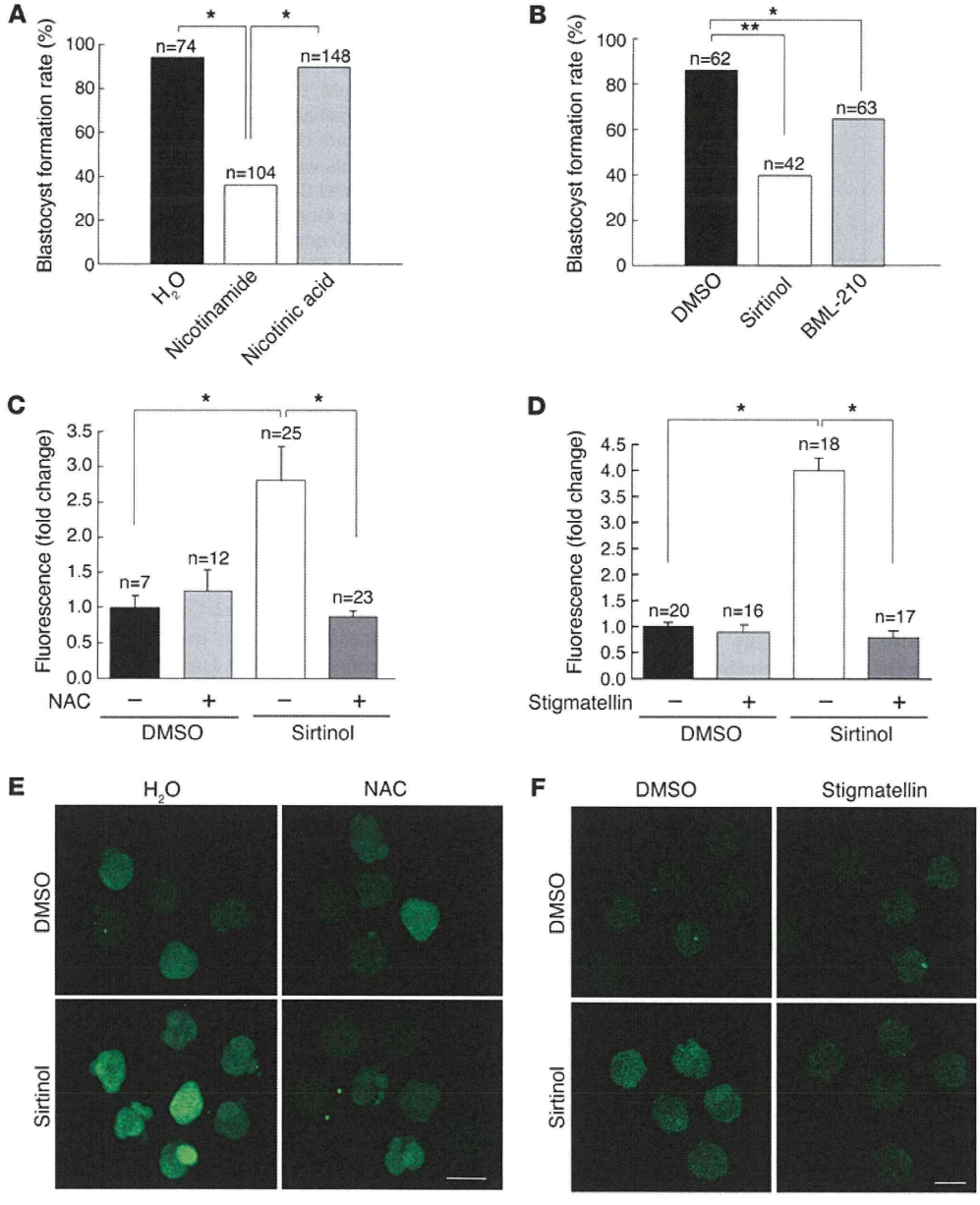

Figure 2

Sirtuin inhibitors cause decreased blastocyst formation and increased mitochondrial ROS generation in preimplantation embryos. (**A** and **B**) The sirtuin inhibitors nicotinamide, sirtinol, and BML-210 caused developmental arrest. Embryos were treated with inhibitors during IVF and in vitro culture, and the blastocyst formation rate was calculated by dividing the number of blastocysts by the number of 2-cell embryos. Nicotinic acid, a nicotinamide derivative, had no effect on developmental outcome. H_2O and DMSO (final concentration, 0.2%) served as control for each experiment. Data are derived from 7 independent experiments. Statistical assessments were performed by applying Ryan's multiple-comparison test. $^*P < 0.05$; $^{**}P < 0.001$. (**C** and **D**) Sirtinol increased intracellular ROS levels, as estimated by CM-H_2DCFDA fluorescence intensity. This increase was blocked by NAC (**C**) and stigmatellin (**D**). Embryos were treated with the indicated agents for 72 hours. Quantitative data of fluorescence intensity, obtained using ImageJ, were standardized by dividing each value by the average value of the control group in each experiment. Data are derived from 3 independent experiments. Statistical assessments were performed by applying Games-Howell test. $^*P < 0.05$. (**E** and **F**) Representative images of CM-H_2DCFDA fluorescence in embryos analyzed in **C** and **D**, respectively. Scale bars: 100 μm.

some cell types (25). To examine whether Sirt3 localizes to mitochondria in preimplantation embryos, we injected in vitro–transcribed Sirt3-EGFP mRNA into fertilized eggs and observed EGFP fluorescence at the 2-cell stage. The distribution pattern of Sirt3-EGFP fusion protein was granular within the cytoplasm (Figure 4A). Costaining with MitoTracker showed colocalization of Sirt3-EGFP to mitochondria, as expected (Figure 4, B and C). In contrast, Sirt1-EGFP (Figure 4, D–F) and Sirt2-EGFP (Figure 4, G–I) were localized to the nucleus and cytoplasm, respectively. EGFP alone was distributed throughout the cell (Figure 4J). These results indicate that Sirt3 is likely to be localized to mitochondria in mouse preimplantation embryos.

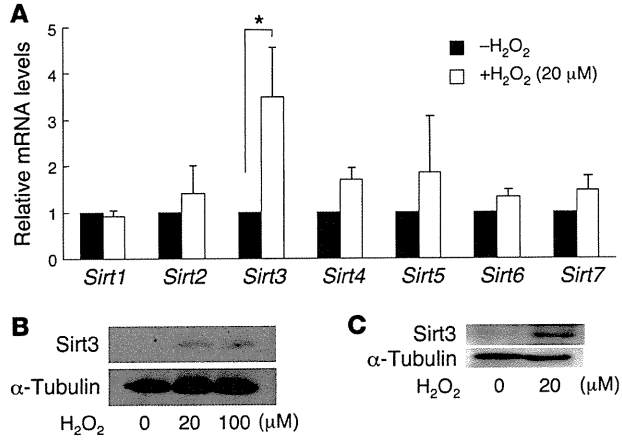

Figure 3
Oxidative stress upregulates the expression of sirtuins. (**A**) Quantitative real-time RT-PCR analysis of sirtuin gene expression after H_2O_2 treatment (20 μM, 6 hours) in preimplantation embryos. *Sirt3* mRNA levels were significantly increased in 4-cell embryos after exposure to H_2O_2. Data are derived from 3 independent experiments. Statistical assessments were performed by applying Mann-Whitney *U* test. $^*P < 0.05$. (**B** and **C**) Western blotting analysis showing Sirt3 protein upregulation in 4-cell embryos (**B**) and NIH 3T3 cells (**C**) after H_2O_2 treatment (**B**, 20 and 100 μM, 18 hours; **C**, 20 μM, 24 hours) detected by Western blot. Blotting for α-tubulin served as an internal control.

RNAi-mediated Sirt3 knockdown increases mitochondrial ROS generation, causing developmental arrest in preimplantation embryos. To investigate the role of Sirt3 in preimplantation development, we selectively knocked down the expression of Sirt3 by injecting Sirt3-targeted siRNA into fertilized eggs. We designed 2 stealth siRNAs to target 2 different regions of the Sirt3 transcript (siRNAs 1 and 2; see Methods and Supplemental Table 2). Both siRNAs downregulated Sirt3 mRNA and protein in NIH 3T3 cells (Supplemental Figure 3, A and B), and the efficacy was confirmed in 8-cell to morula stage embryos (Supplemental Figure 3, C and D). The expression of other sirtuin family members was not affected by Sirt3 siRNA (Supplemental Figure 3E).

We next examined whether Sirt3 knockdown increases intracellular ROS levels by using CM-H_2DCFDA fluorescence dye. In Sirt3 siRNA–injected embryos, CM-H_2DCFDA fluorescence was significantly higher than that in control embryos (Figure 5, A–D). This increase in fluorescence intensity was abolished by NAC (Figure 5, A and C) and stigmatellin (Figure 5, B and D), as in sirtinol-treated embryos. Apocynin, a selective inhibitor of NAD(P)H oxidase, also partially suppressed this increase, but the effect was less than that of stigmatellin (Figure 5, B and D). These results suggest that Sirt3 inactivation may cause intracellular ROS production, mainly of mitochondrial origin.

Embryos injected with either of the stealth Sirt3 siRNAs exhibited a significant decrease in blastocyst formation rate, whereas fertilization rate, estimated by the formation of 2-cell embryos, was not affected (Figure 6A and Supplemental Figure 4). This decrease in blastocyst formation was suppressed by NAC (Figure 6B), which indicates that increased ROS is possibly responsible for developmental arrest in Sirt3-knockdown embryos.

Sirt3 knockdown–induced developmental defects are abolished in low-oxygen conditions. The results of our Sirt3-knockdown experiments suggested that in vitro culture conditions are stressing the embryos to induce increased ROS and developmental defects in the absence of sufficient Sirt3 activity. To test this possibility, we performed the same experiments under low-oxygen (5% O_2) conditions. As expected, Sirt3 knockdown did not affect 2-cell and blastocyst formation rates in low-oxygen conditions (Figure 7A). Sirt3 knockdown–induced increase in intracellular ROS levels was also abolished in low-oxygen conditions (Figure 7, B and C). These results indicate that Sirt3 may play a protective role for preimplantation embryos within a stressful environment.

Sirt3-null eggs are defective in developmental competence after IVF and parthenogenesis. To confirm the results from siRNA-knockdown experiments, we performed similar experiments using embryos genetically deficient in Sirt3. Gametes with the *Sirt3*$^+$ or *Sirt3*$^-$ allele were prepared from *Sirt3*$^{+/+}$ and *Sirt3*$^{-/-}$ littermates, respectively, and were subjected to IVF. Unlike Sirt3 siRNA–injected embryos, fertilization rate significantly decreased in embryos derived from *Sirt3*$^-$ eggs, regardless of paternal genotype (Table 1). This difference may be explained by the lack of maternally derived Sirt3 storage in *Sirt3*$^-$ eggs. In addition, blastocyst formation rate under in vitro culture conditions was also significantly decreased in embryos derived from *Sirt3*$^-$ eggs (Table 2). These results indicate that Sirt3 of maternal origin plays an important role in fertilization and preimplantation development under in vitro conditions.

The role of maternally derived Sirt3 in preimplantation development was further confirmed by examining development of parthenogenetic embryos with different Sirt3 levels. Eggs injected with Sirt3 and control siRNA developed to the 2-cell stage after parthenogenetic activation by $SrCl_2$ (Sr^{2+}) at comparable rates (Figure 8A). Conversely, blastocyst formation was significantly compromised in parthenogenetic embryos injected with Sirt3 siRNA (Figure 8A). Similar results were obtained using eggs with the *Sirt3*$^+$ or *Sirt3*$^-$ alleles. Parthenogenetically activated embryos deficient in Sirt3 developed well to the 2-cell stage, but their blastocyst formation rates decreased (Figure 8B). These results confirmed the importance of maternally derived Sirt3 for preimplantation developmental competence.

Long-term in vitro culture leads to defective postimplantation development in Sirt3-knockdown embryos. In contrast to our present finding, *Sirt3*$^{-/-}$ mice have previously been shown to be healthy under basal conditions and fertile (31). However, another group has reported that cells from *Sirt3*$^{-/-}$ mice exhibit reduced basal ATP levels and increased acetylation of mitochondrial proteins (30). Therefore, we speculated that Sirt3 might not be required for development under natural optimal conditions, but functions under stressful conditions, such as in vitro culture. To explore this possibility, we transferred siRNA-injected embryos to pseudopregnant mice after short- or long-term in vitro culture and assessed the implantation rate and postimplantation survival of Sirt3-knockdown embryos. When embryos were transferred at the 2-cell stage, the rates of implantation and full-term survival were not significantly affected by Sirt3 knockdown (Figure 9, A and B). Conversely, implantation rate and full-term survival were significantly decreased in Sirt3

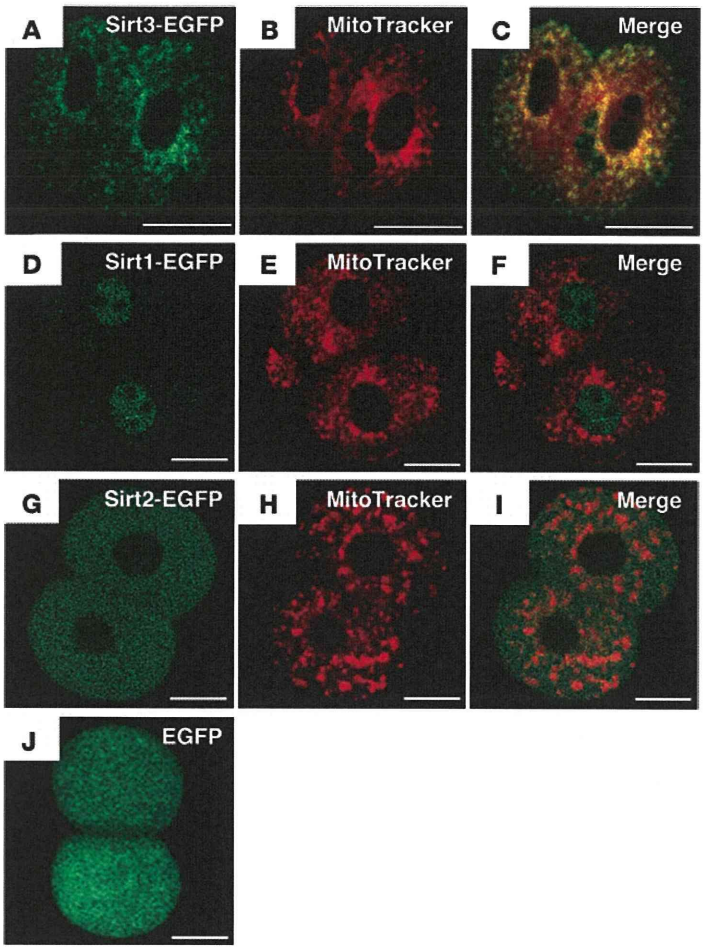

Figure 4
Confocal imaging analysis of the localization of sirtuin-EGFP fusion proteins in preimplantation embryos. Intracellular injection of mRNA coding Sirt3-EGFP (**A–C**), Sirt1-EGFP (**D–F**), Sirt2-EGFP (**G–I**), or EGFP alone (**J**) was performed at the pronuclear stage, and the EGFP signals (**A**, **D**, **G**, and **J**; green) were observed at the 2-cell stage. (**B**, **E**, and **H**) Mitochondria were stained by MitoTracker (red) just 15 minutes before observation. (**C**, **F**, and **I**) Colocalization of Sirt3-EGFP signals to MitoTracker staining confirmed mitochondrial localization of Sirt3. Scale bars: 20 μm.

siRNA–treated embryos when transferred at the morula/blastocyst stage, 72–96 hours after siRNA injection (Figure 9, A and B). These results suggest that Sirt3 is required for embryos to establish a successful pregnancy after long-term in vitro culture.

p53 is involved in developmental arrest due to Sirt3 deficiency. Increased intracellular ROS is known to trigger the activation of the tumor suppressor p53, leading to cell cycle arrest and apoptosis in various cell types (35, 36). Many functions of p53 are attributed to its transcriptional activity on various gene promoters, including that of the cyclin-dependent kinase inhibitor p21 (37, 38). Recently, p53 has been reported to induce the differentiation of ES cells by suppressing the expression of Nanog homeobox (*Nanog*), a transcription factor required for ES cell self-renewal, after DNA damage (39, 40). To investigate whether p53 is involved in developmental arrest in Sirt3-knockdown or knockout embryos, we examined the levels of p53 and its target gene expression. In *Sirt3*$^{-/-}$ early embryos, *p53* and *p21* expression was upregulated, whereas *Nanog* expression was downregulated (Figure 10A and Supplemental Figure 5A). Similar expression patterns were recapitulated by treatment with H_2O_2 in wild-type embryos (Figure 10A and Supplemental Figure 5A). Involvement of p53 was further investigated using siRNA-mediated knockdown (Supplemental Table 2). Injection of both control and Sirt3 siRNA appeared to increase *p53* mRNA to a similar level, possibly as a result of stimuli caused by the microinjection procedure (Figure 10B and Supplemental Figure 5B). Treatment with NAC decreased *p53* mRNA levels only in control siRNA–injected embryos, revealing a difference in *p53* expression between control and Sirt3 siRNA embryos similar to that between wild-type and *Sirt3*$^{-/-}$ embryos (Figure 10B and Supplemental Figure 5B). In contrast, p53 protein levels were increased in Sirt3-knockdown embryos without NAC treatment (Figure 10C), which indicates that p53 protein is stabilized in Sirt3-knockdown embryos. Accordingly, *p21* expression was upregulated and *Nanog* was downregulated, as observed in *Sirt3*$^{-/-}$ embryos (Figure 10B and Supplemental Figure 5B). These effects were suppressed by NAC (Figure 10B and Supplemental Figure 5B), which indicates that p53 is stabilized and activated by ROS in Sirt3-knockdown embryos.

Finally, we examined the effect of siRNA-mediated p53 knockdown on development of Sirt3-knockdown embryos to test whether the increased p53 is involved in developmental arrest caused by Sirt3 deficiency. Coinjection with p53 siRNA effectively downregulated *p53* and *p21* expression and upregulated *Nanog* expression in Sirt3 siRNA–injected embryos (Figure 10D and Supplemental Figure 5C). Furthermore, the rate of blastocyst formation was significantly improved in Sirt3-knockdown embryos by coinjection with p53 siRNA (Figure 10E). These results indicate that ROS-induced p53 activation contributes to developmental arrest in Sirt3-knockdown embryos under in vitro culture conditions.

Discussion

In the present study, we demonstrated the involvement of sirtuins, especially Sirt3, in mouse preimplantation development. Early expression patterns and developmental arrest by sirtuin inhibitors suggest the involvement of this protein family in preimplantation development. Among them, Sirt3, predominantly of maternal origin, was shown to be required for in vitro preimplantation development by experiments using siRNA-induced knockdown and gene-knockout mice. In apparent contrast to previous studies reporting that *Sirt3*-deficient mice demonstrate no obvious phenotype in fertility, although they show mitochondrial protein hyperacetylation and reduction in basal ATP levels (30, 31), our present findings indicate that the *Sirt3*-null phenotype becomes evident when embryos are exposed to stress conditions. In IVF and in vitro–cultured embryos, Sirt3 inactivation caused increased ROS production, which led to p53 activation and subsequent developmental arrest. Collectively, our present results identified Sirt3 as one of the key factors determining the developmental outcome of IVF embryos, at least in mice.

Maternal and zygotic expression of sirtuins in eggs and preimplantation embryos. All sirtuins were expressed in eggs, and the expression levels gradually decreased during preimplantation development, which indicated that they were transcribed and stored

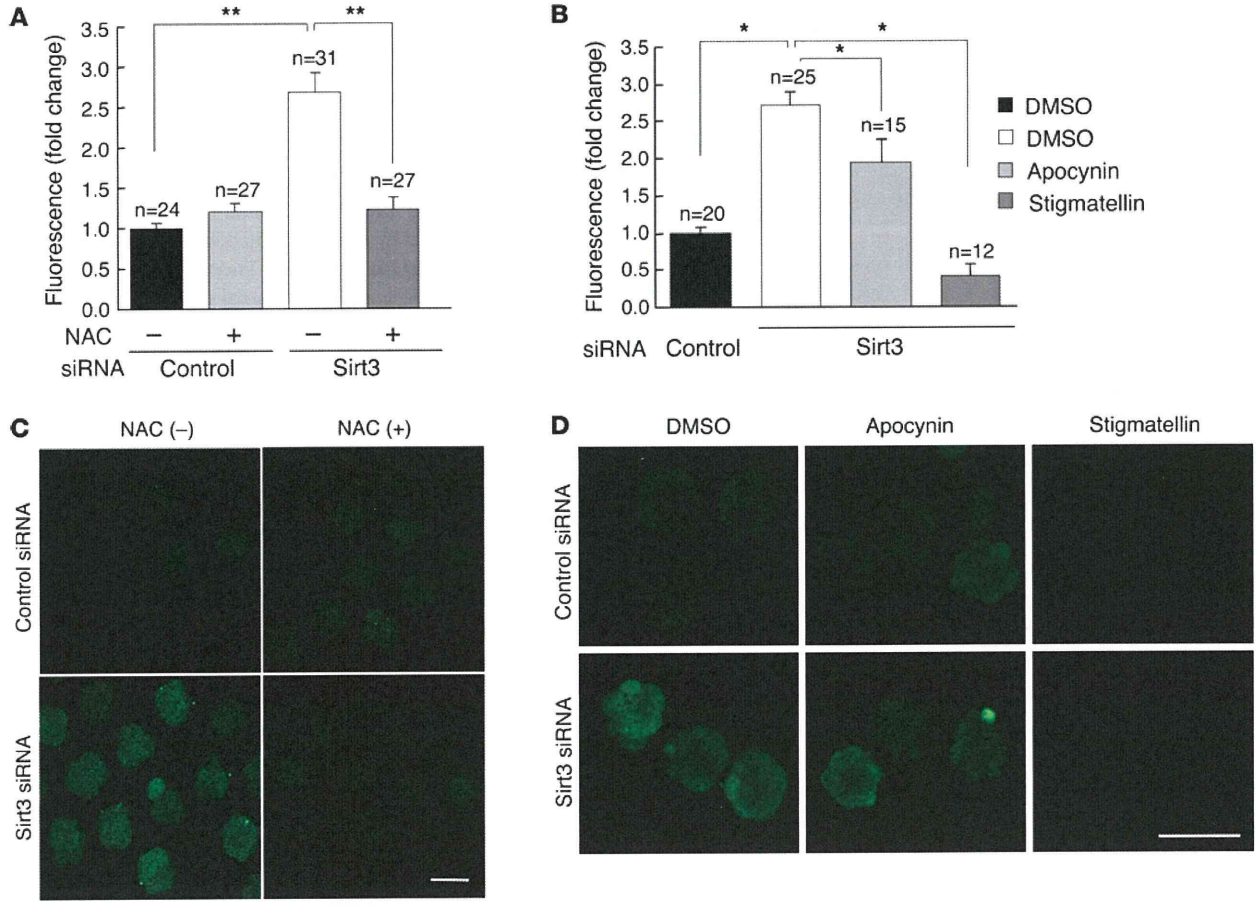

Figure 5

Sirt3 knockdown increases intracellular ROS, mainly of mitochondrial origin, in preimplantation embryos. (**A** and **B**) Injection of Sirt3 siRNA increased intracellular ROS levels, as estimated by CM-H_2DCFDA fluorescence intensity. This increase was abolished by NAC (**A**) and stigmatellin (**B**), but was only partially decreased by apocynin (**B**). Embryos were injected with control or Sirt3 siRNA at the pronuclear stage and were cultured with or without NAC for 72 hours. To identify the major origin of increased intracellular ROS, embryos were treated with apocynin or stigmatellin for 30 minutes before CM-H_2DCFDA staining. Quantitative data of fluorescence intensity, obtained using ImageJ, were standardized by dividing each value by the average value of the control group in each experiment. Data are derived from 3 (**A**) or 4 (**B**) independent experiments. Statistical assessments were performed by applying Games-Howell test. $^*P < 0.05$; $^{**}P < 0.001$. (**C** and **D**) Representative images of CM-H_2DCFDA fluorescence in embryos analyzed in **A** and **B**, respectively. Scale bars: 100 μm.

during the process of oogenesis but their zygotic expression was relatively low or undetectable. In contrast, the expression of some sirtuins, including Sirt3, was upregulated by oxidative stress in zygotes. This is in agreement with previous reports that Sirt3 is a stress-responsive deacetylase in other cell types (41). Although the mechanism of the stress-induced upregulation is unclear, this finding suggests that zygotic expression of some sirtuin genes can be induced in stress conditions. However, the developmental competence of *Sirt3*-null eggs after IVF was reduced regardless of the sperm genotype. Thus, we conclude that maternally derived Sirt3 is critical for normal preimplantation development after IVF, whereas zygotically activated Sirt3 is not sufficient to compensate the loss of maternal Sirt3.

Regulation of mitochondrial ROS generation by Sirt3. Sirt3 is regarded as the major mitochondrial deacetylase involved in the regulation of energy metabolism (19–21). Mitochondria are not only the site of oxidative phosphorylation and energy production, but also a major source of ROS. Excessive ROS generation caused by mitochondrial dysfunction leads to oxidative stress, which is implicated in pathophysiological processes such as genomic instability and aging (42). In preimplantation development, mitochondrial dysfunction and subsequent ROS-induced oxidative stress have been shown to adversely affect developmental outcome (9, 18), indicating the importance of protective mechanisms against excessive ROS generation. The present study has shown that Sirt3-knockdown preimplantation embryos exhibited an increase in intracellular ROS, mainly of mitochondrial origin. This finding is complementary to previous studies demonstrating that overexpression of wild-type Sirt3 decreased intracellular ROS, whereas overexpression deacetylase-defective mutant Sirt3 increased it (27, 43). In addition, decreased blastocyst formation rates were improved by the antioxidant NAC, which indicated that the increase in ROS was responsible for developmental arrest. Furthermore, lowering oxygen concentration in culture